Heavy-ion physics for beginners (I)

Wojciech Florkowski[1,2]

[1] Jan Kochanowski University, Kielce, Poland
[2] Institute of Nuclear Physics, Polish Academy of Sciences, Kraków, Poland

International Conference on New Frontiers in Physics
10-16 June 2012 Kolymbari, Crete, Greece

Outline

Outline

STANDARD MODEL (MODULES) of HEAVY–ION COLLISIONS

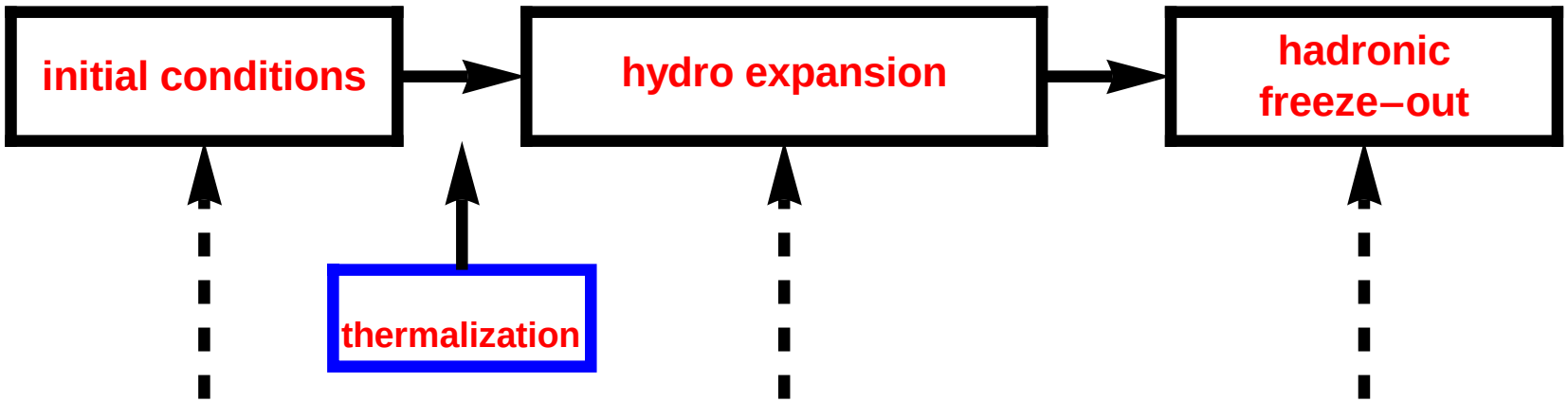

NEW: FLUCTUATIONS IN THE INITIAL STATE / EVENT–BY–EVENT HYDRO / FINAL–STATE FLUCTUATIONS

EQUATION OF STATE?

VISCOSITY?

1. INTRODUCTION

1.1 High-energy nuclear collisions

Physics of the ultra-relativistic heavy-ion collisions is an **interdisciplinary field** which connects the **high-energy physics of elementary particles** with the **nuclear physics**. There exist also connections to **astrophysics** and **cosmology**.

The name **"heavy-ions"** is used for heavy atomic nuclei, whereas the term **"ultra-relativistic energy"** denotes the energy regime where the kinetic energy exceeds significantly the rest energy (I use natural units where $c = \hbar = k_B = 1$).

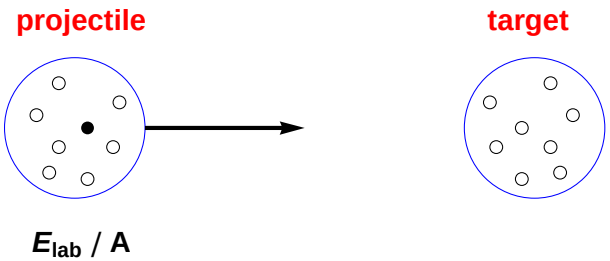

$$E_{\rm lab}/A \gg m_{\rm N} \sim 1 \text{ GeV}. \quad (1)$$

$E_{\rm lab}$ – energy in the lab, A – atomic number, $m_{\rm N}$ – nucleon mass.

In the case of colliders, we speak more often about the energy in the center-of-mass frame per nucleon pair.

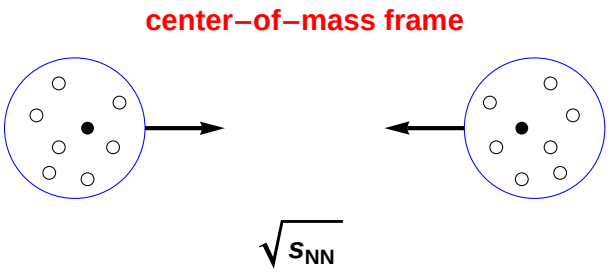

$$\sqrt{s_{\rm NN}} \gg m_{\rm N} \sim 1 \text{ GeV}. \quad (2)$$

1.1 High-energy nuclear collisions

In 2000 the first data from the **Relativistic Heavy Ion Collider (RHIC)** at BNL were collected. During the first run, the maximum energy of 130 GeV per nucleon pair was achieved. In the next years new runs took place with the maximum energy of 200 GeV per nucleon pair. One of those runs was devoted to the study of the deuteron-gold collisions which were analyzed in order to get the proper reference point for the more complicated gold on gold collisions.

Satellite view of RHIC and BNL (Long Island, New York, USA).

1.1 High-energy nuclear collisions

The main activity in the field is connected now with **Large Hadron Collider (LHC)** at CERN (Pb on Pb reactions at $\sqrt{s_{\rm NN}}$ = 2.76 TeV, start Nov.-Dec., 2010).

Aerial view of CERN and Geneva (Switzerland).

Nevertheless, the performance of new experiments at lower energies is also very important, since this allows us to study the energy dependence of many characteristics of the particle production, and direct searches for new phenomena, **NA61** at CERN, **STAR** at BNL.

1.2 Theoretical methods

In the ultra-relativistic heavy-ion collisions very large numbers of particles are produced (we deal with so called large particle **multiplicities**).

For example, in the central Au+Au collisions at RHIC, at the highest beam energy $\sqrt{s_{\mathrm{NN}}}$ = 200 GeV, the total charged particle multiplicity is about 5000. Hence, the number of produced particles exceeds the number of initial nucleons by a factor of 10.

In this situation, different theoretical methods are used, which are suitable for description of large macroscopic systems, e.g., **thermodynamics, hydrodynamics, kinetic (transport) theory, field theory at finite temperature and density, non-equilibrium field theory, Monte-Carlo simulations**.

... we also know the underlying fundamental theory!

1.3 Quantum Chromodynamics: asymptotic freedom

Feynman and Bjorken argued that high-energy experiments should reveal the existence of partons, i.e., particles that are parts of hadrons, suggestions spectacularly verified in the **deep inelastic scattering** of electrons on protons, the experiments carried out at the Stanford Linear Accelerator Center (SLAC) in 1969. The partons were identified with quarks.

1973 – the discovery of **asymptotic freedom** in the strong interactions by Gross, Politzer, and Wilczek allowed for making precise predictions of the results of many high-energy experiments in the framework of the perturbative quantum field theory — the asymptotic freedom is the property that the **interaction between particles becomes weaker at shorter distances**.

1975 – Collins and Perry argued that “superdense matter (found in neutron-star cores, exploding black holes, and the early big-bang universe) consists of quarks rather than of hadrons”.

1.3 Quantum Chromodynamics

1975 – Cabibbo and Parisi identified the limiting Hagedorn temperature with the temperature of the phase transition from hadronic to quark matter, they also sketched the first phase diagram of strongly interacting matter.

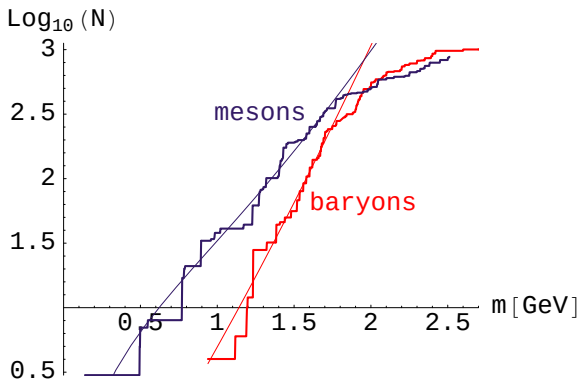

Hadron mass spectrum grows like e^{m/T_H} where T_H is the Hagedorn temperature, in this case there is a limiting temperature for hadrons, integrals over m of the expressions such as $e^{m/T_H - \sqrt{m^2+p^2}/T}$ diverge if $T \geq T_H$!

W. Broniowski and WF, different T_H for baryons and mesons (see figure)

$T \to \infty$, density grows like T^3, inter-particle distance $\sim 1/T \to 0$, weakly interacting system!

Gauge theories at finite temperature:
Kislinger and Morley (1975), Freedman and McLerran (1976),
Shuryak introduced in 1978 the name **quark-gluon plasma (QGP)**,
Kapusta (1979), ...

1.3 Quantum Chromodynamics: confinement

Probably the most striking feature of QCD is the **color confinement**, which is the other side of the asymptotic freedom. This is the phenomenon that color charged particles (such as quarks and gluons) cannot be isolated as separate objects. In other words, quarks and gluons cannot be directly observed. The physical concept of confinement may be illustrated by a string which is spanned between the quarks when we try to separate them. If the quarks are pulled apart too far, large energy is deposited in the string which breaks into smaller pieces.

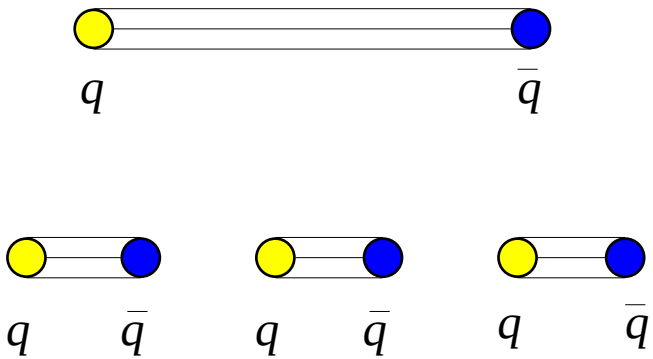

1.4 Quark-gluon plasma

The main challenge of the ultra-relativistic heavy-ion collisions is the observation of the **deconfinement phase transition**.

As we have mentioned above, at Earth conditions (i.e., at low energy densities) quarks and gluons are confined in hadrons. However, **with increasing temperature (heating) and/or increasing baryon density (compression), a phase transition may occur to the state where the ordinary hadrons do not exist anymore; quarks and gluons become the proper degrees of freedom, and their motion is not confined to hadrons**.

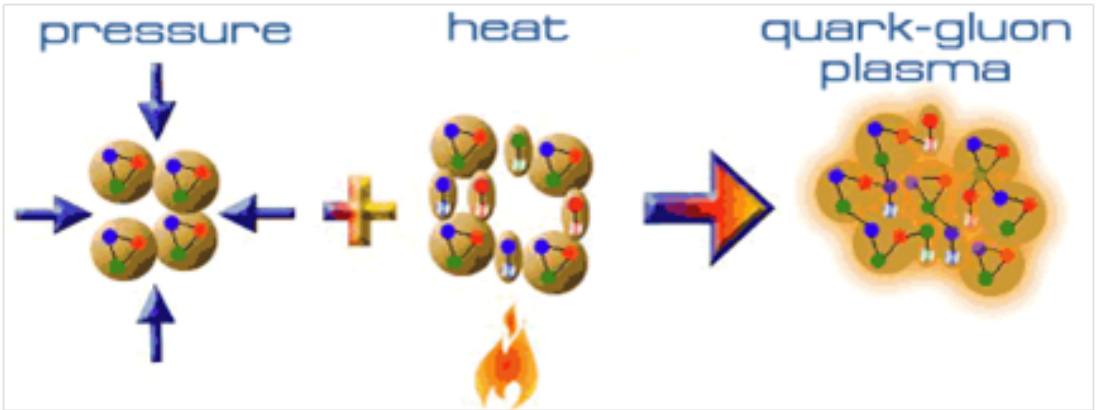

1.4 Quark-gluon plasma: equation of state

massless gluons (Stefan-Boltzmann's law)

$$\varepsilon_g = 16\,\frac{\pi^2}{30}\,T^4, \qquad P_g = \frac{1}{3}\,\varepsilon_g$$

massless quarks

$$\varepsilon_q + \varepsilon_{\overline{q}} = 6N_f\left(\frac{7\pi^2}{120}\,T^4 + \frac{1}{4}\,\mu^2 T^2 + \frac{1}{8\pi^2}\,\mu^4\right),$$

$$P_q + P_{\overline{q}} = \frac{1}{3}\left(\varepsilon_q + \varepsilon_{\overline{q}}\right)$$

μ is one third of the baryon chemical potential μ_B, $\mu = \frac{1}{3}\mu_B$
WEAKLY INTERACTING GAS of quarks and gluons, B – bag constant

$$\varepsilon_{\rm qgp} = \varepsilon_g(T) + \varepsilon_q(T,\mu) + \varepsilon_{\overline{q}}(T,\mu) + B$$

or

$$P_{\rm qgp} = P_g(T) + P_q(T,\mu) + P_{\overline{q}}(T,\mu) - B$$

1.4 Quark-gluon plasma: naive phase transition

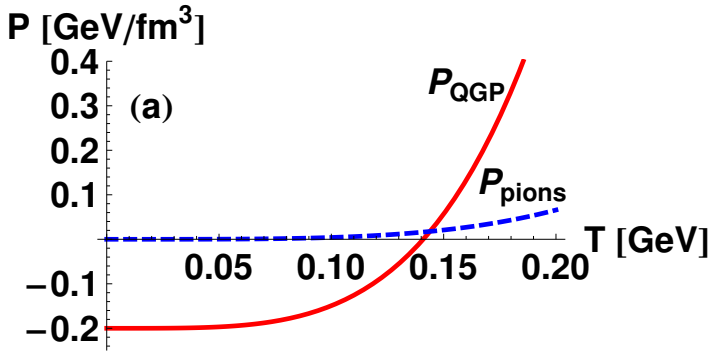

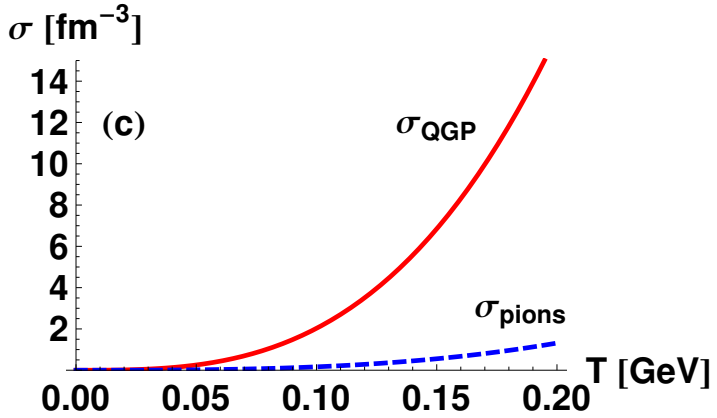

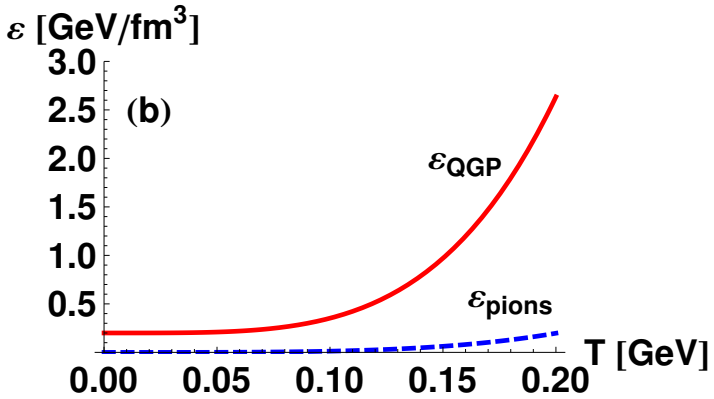

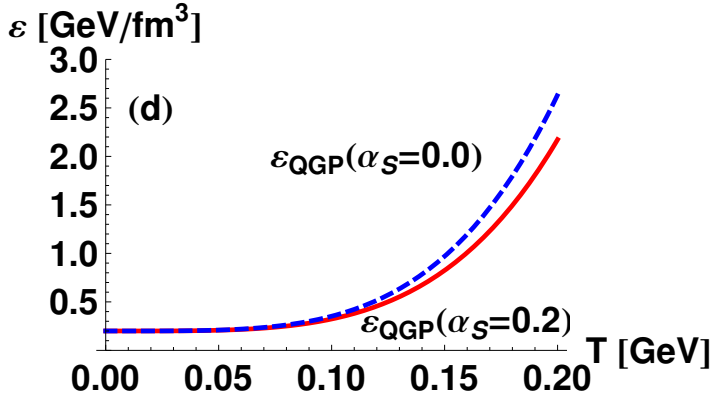

first order phase transition between a weakly interacting plasma and a pion gas

1.4 Quark-gluon plasma: lattice QCD simulations

Calculations done at zero baryon chemical potential, $\mu_B = 0$!
sound velocity $c_s^2(T) = \frac{\partial P}{\partial \varepsilon}$
drops to zero at the first order phase transition
stays large at the **crossover phase transition**

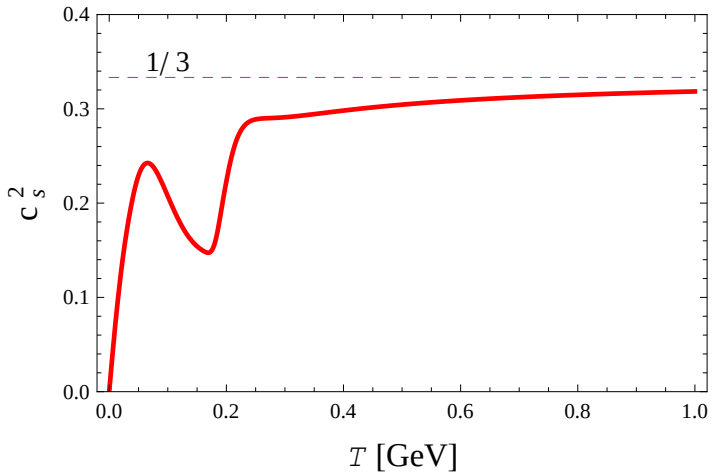

lattice simulations of QCD done by the Budapest-Wuppertal group (Z. Fodor et al.),
figure – connecting hadron-resonance gas with LQCD by M. Chojnacki and WF (2007)

1.4 Quark-gluon plasma: phase diagram

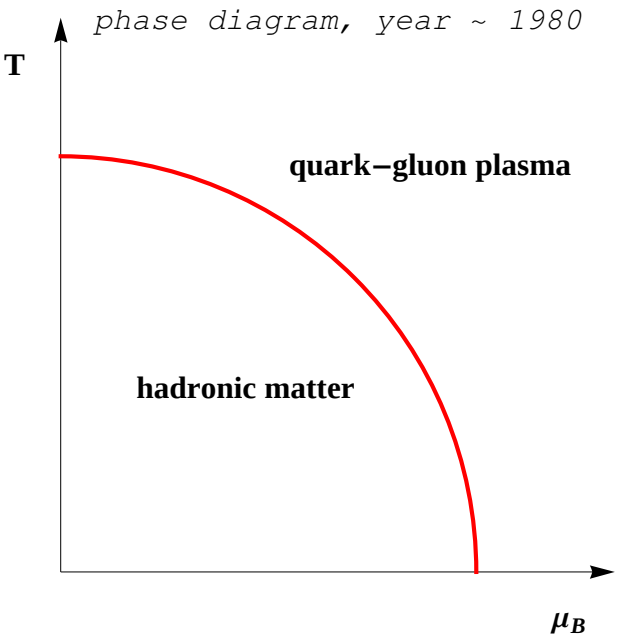

Cabibbo-Parisi

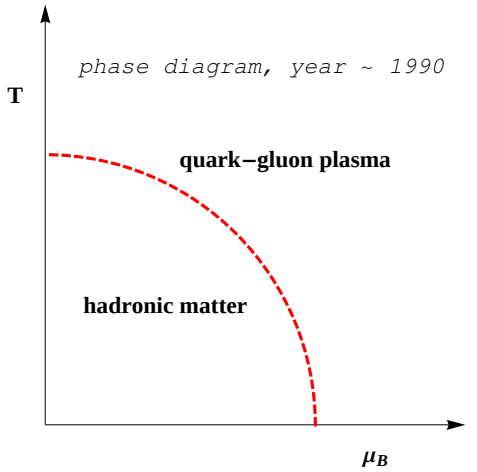

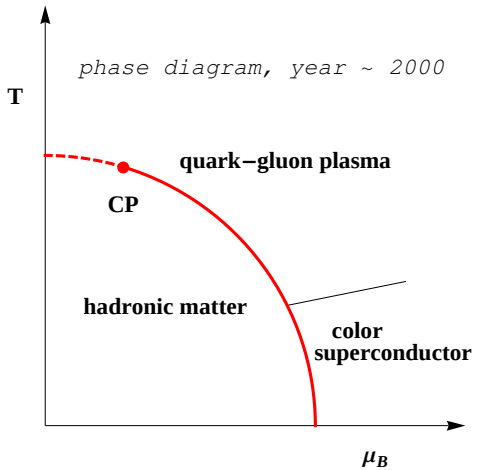

2. BASIC DICTIONARY

2.1 Participants, spectators, and impact parameter

At very high energies, simple geometric concepts are often used, for example, one separates so called participants from spectators — if we assume that all nucleons propagate along parallel, straight line trajectories, then the nucleons which do not meet any other nucleons on their way are called **spectators**. Other nucleons which interact with each other are called **participants**.

The participants which suffered at least one inelastic collision are called the **wounded nucleons**.

A two-dimensional vector connecting centers of the colliding nuclei in the plane transverse to the nucleon trajectories is called the **impact vector**, and its length is the **impact parameter**.

In particle as well as in nuclear physics it is practical to introduce a coordinate system, where the spatial z-axis is parallel to the beam of the accelerator, and where the **impact vector b** points in x-direction. The two axes, x and z, span the **reaction plane** of a given collision.

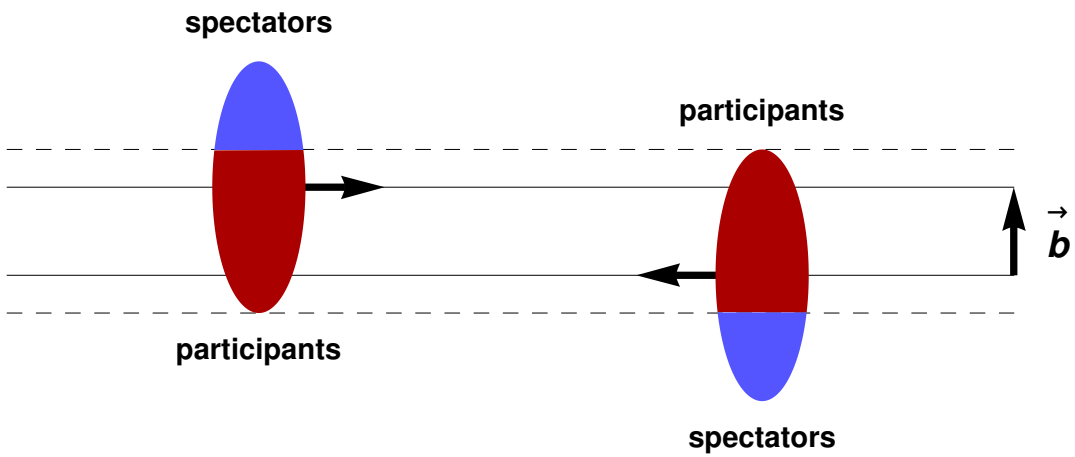

2.2.1 Kinematical variables: transverse mass

The component of a three-vector **A** parallel to z-axis is usually denoted by $\mathbf{A}_{\parallel}$, and the transverse component is $\mathbf{A}_{\perp} = \mathbf{A} - \mathbf{A}_{\parallel}$. The **transverse mass** of a particle is defined as

$$m_{\perp} = \sqrt{m^2 + \mathbf{p}_{\perp}^2}, \tag{3}$$

where m and **p** are the particle's mass and three-momentum [1].

The measured $m_{\perp}$-distribution of the produced particles is typically of the **exponential form** (for not too large transverse momenta, $p_{\perp} < 1$–2 GeV)

$$\frac{dN}{2\pi\, m_{\perp}\, dm_{\perp}} = A \exp\left(-m_{\perp}/\lambda\right). \tag{4}$$

The two parameters A and λ are obtained from the fits to the experimental data.

[1] The "transverse" quantities are sometimes denoted by the subscript T, e.g., m_T or p_T. The "longitudinal" quantities are then denoted by the subscript L, e.g., p_L.

2.2.1 Kinematical variables: transverse mass

The measurements done by the NA49 Collaboration at CERN. The transverse-mass spectra of π^-, K^+, and K^- at midrapidity ($|y| < 0.1$ for kaons and $0 < y < 0.2$ for pions) in the central Pb+Pb collisions at the energy $E_{\rm lab} = 40$ A GeV (triangles), 80 A GeV (squares), and 158 A GeV (circles). The lines are the exponential fits to the spectra in the interval 0.2 GeV $< m_T - m <$ 0.7 GeV. The values for 80 A GeV and 158 A GeV are rescaled by the factors of 10 and 100, respectively.

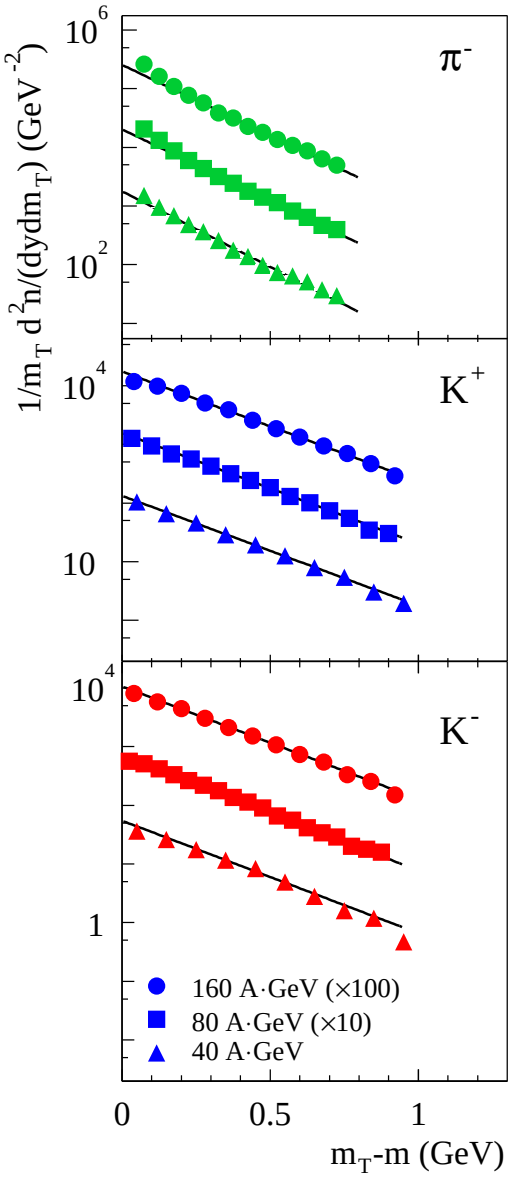

2.2.2 Kinematical variables: rapidity

Since we deal with relativistic energies, it is useful to use the **rapidity** instead of the standard velocity

$$\mathrm{y} = \frac{1}{2} \ln \frac{(E+p_{\parallel})}{(E-p_{\parallel})} = \operatorname{arctanh}\left(\frac{p_{\parallel}}{E}\right) = \operatorname{arctanh}\left(\mathrm{v}_{\parallel}\right). \tag{5}$$

Here E is the energy of a particle, $E = \sqrt{m^2 + \mathbf{p}^2}$, and $\mathrm{v}_{\parallel} = p_{\parallel}/E$ is the longitudinal component of the velocity. **Rapidity is additive under Lorentz boosts along the z-axis.**

Using the rapidity and the transverse mass, we can calculate the energy and the longitudinal momentum of a particle from the equations

$$E = p^0 = m_{\perp} \cosh \mathrm{y} \tag{6}$$

and

$$p_{\parallel} = m_{\perp} \sinh \mathrm{y}. \tag{7}$$

2.2.2 Kinematical variables: rapidity

The measurements done by the NA49 Collaboration at CERN. The rapidity distributions of π^-, K^+, and K^- in the central Pb+Pb collisions at the energy $E_{\rm lab} = 40$ A GeV, 80 A GeV, and 158 A GeV. The closed symbols indicate the measured points, whereas the open points are reflection of the measured points with respect to the axis $\mathrm{y} = 0$.

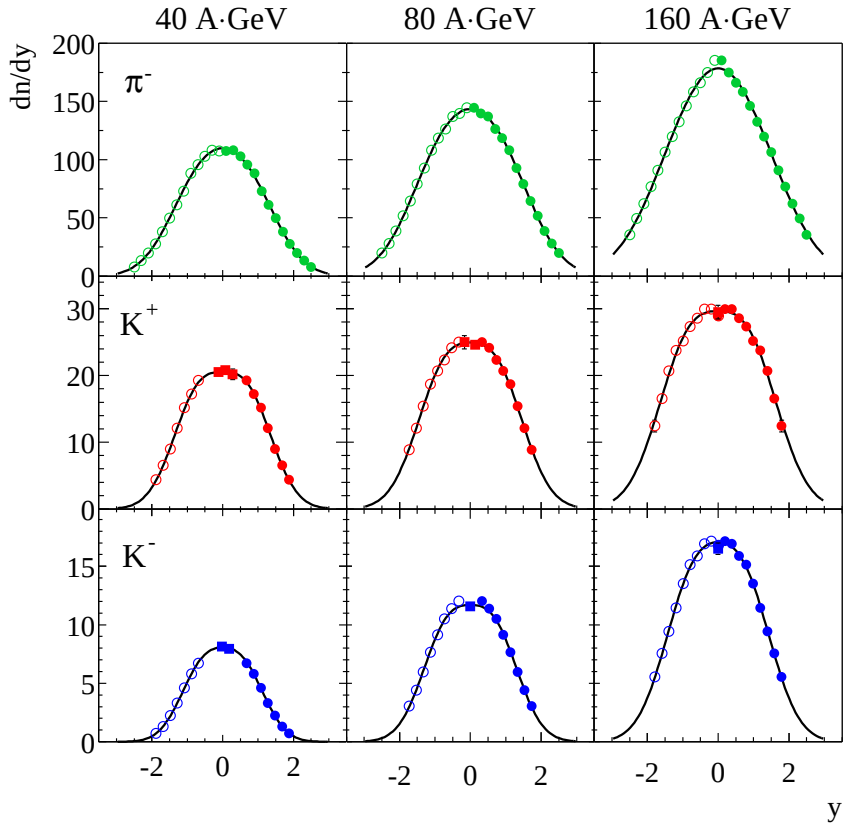

2.2.2 Kinematical variables: rapidity

The measurement of the BRAHMS Collaboration at BNL (Au+Au collisions at $\sqrt{s_{\rm NN}} = 200$ GeV, the most central events). Rapidity distributions **(a)** and average transverse momenta **(b)** of charged pions, charged kaons, protons and antiprotons.

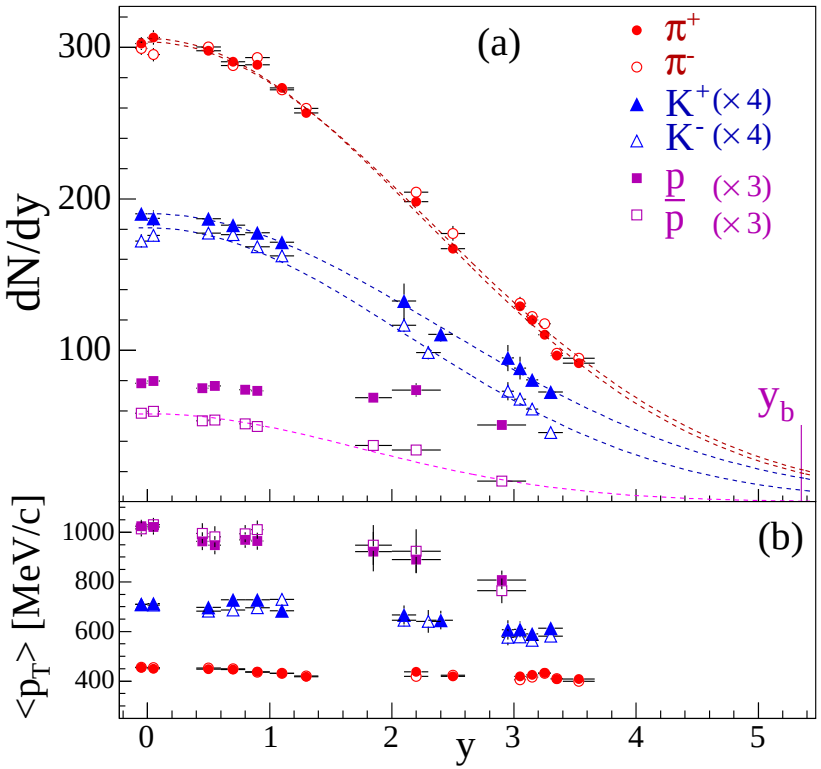

2.2.2 Kinematical variables: pseudorapidity

In the similar way one defines the **pseudorapidity** variable η, namely

$$\eta = \frac{1}{2} \ln \frac{(|\mathbf{p}|+p_{\parallel})}{(|\mathbf{p}|-p_{\parallel})} = \ln\left(\cot\frac{\theta}{2}\right) = -\ln\left(\tan\frac{\theta}{2}\right), \tag{8}$$

where θ is the **scattering angle**. In analogy to Eqs. (6) and (7) we have

$$|\mathbf{p}| = p_{\perp} \cosh\eta \tag{9}$$

and

$$p_{\parallel} = p_{\perp} \sinh\eta. \tag{10}$$

2.2.2 Kinematical variables: pseudorapidity

Pseudorapidity distributions of the charged particles measured by the PHOBOS Collaboration in Au+Au collisions at $\sqrt{s_{\mathrm{NN}}}$ = 130 GeV. The measurements were done for six different centrality classes (the latter will be defined precisely below).

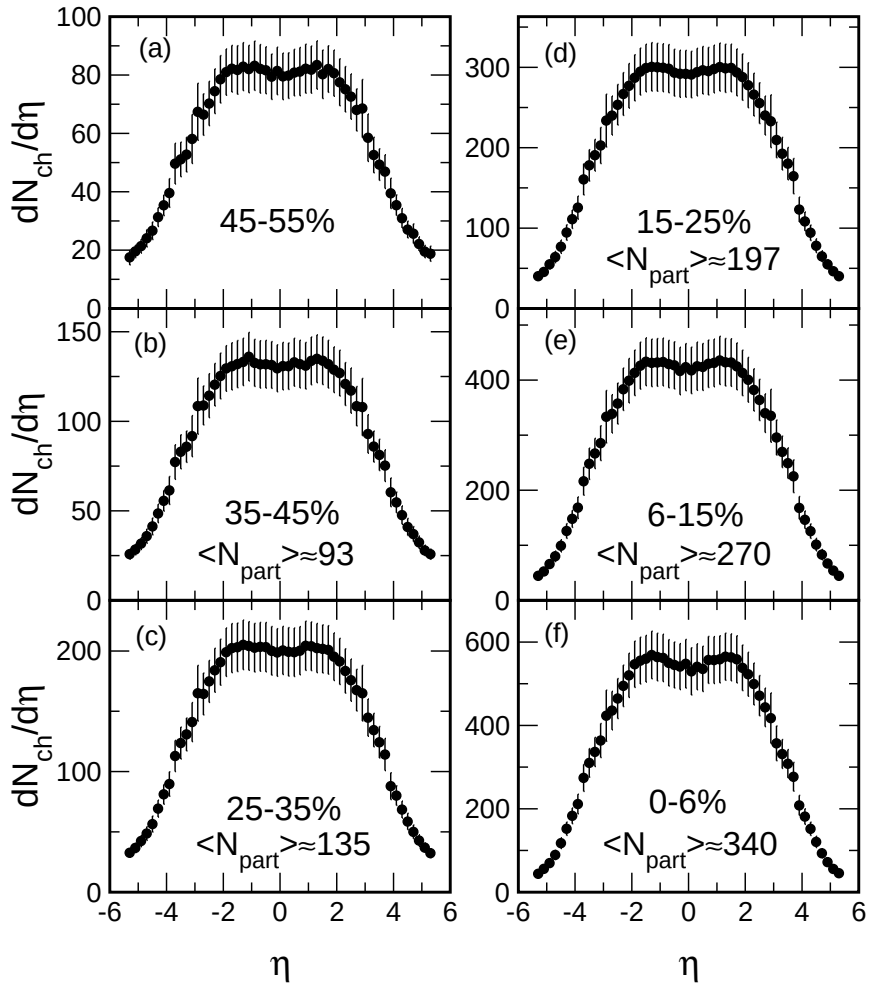

2.2.2 Kinematical variables: rapidity vs. pseudorapidity

In the limit $m \longrightarrow 0$, the rapidity and the pseudorapidity become equal. For finite masses the relations between the rapidity and the pseudorapidity are more complicated

$$y = \frac{1}{2} \ln \left[\frac{\sqrt{p_\perp^2 \cosh^2 \eta + m^2} + p_\perp \sinh \eta}{\sqrt{p_\perp^2 \cosh^2 \eta + m^2} - p_\perp \sinh \eta} \right], \tag{11}$$

$$\eta = \frac{1}{2} \ln \left[\frac{\sqrt{m_\perp^2 \cosh^2 y - m^2} + m_\perp \sinh y}{\sqrt{m_\perp^2 \cosh^2 y - m^2} - m_\perp \sinh y} \right]. \tag{12}$$

Equations (11) or (12) can be used to find a connection between the rapidity distribution of particles and the pseudorapidity distribution

$$\frac{dN}{d\eta\, d^2p_\perp} = \sqrt{1 - \frac{m^2}{m_\perp^2 \cosh^2 y}}\, \frac{dN}{dy\, d^2p_\perp} = \frac{|\mathbf{p}|}{E} \frac{dN}{dy\, d^2p_\perp}. \tag{13}$$

2.2.2 Kinematical variables: central rapidity region

In the center-of-mass frame, the region of the phase-space where $y \approx \eta \approx 0$ is called the **central rapidity region** or the **midrapidity region**. On the other hand, the regions corresponding to the initial rapidities of the projectile and target ($y \approx y_P$, $y \approx y_T$) are called the projectile and target **fragmentation regions**, respectively.

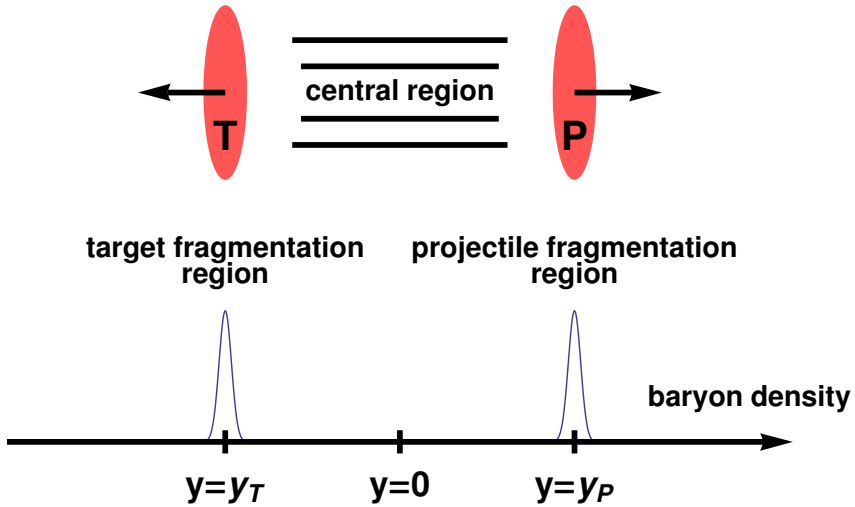

2.3 Centrality

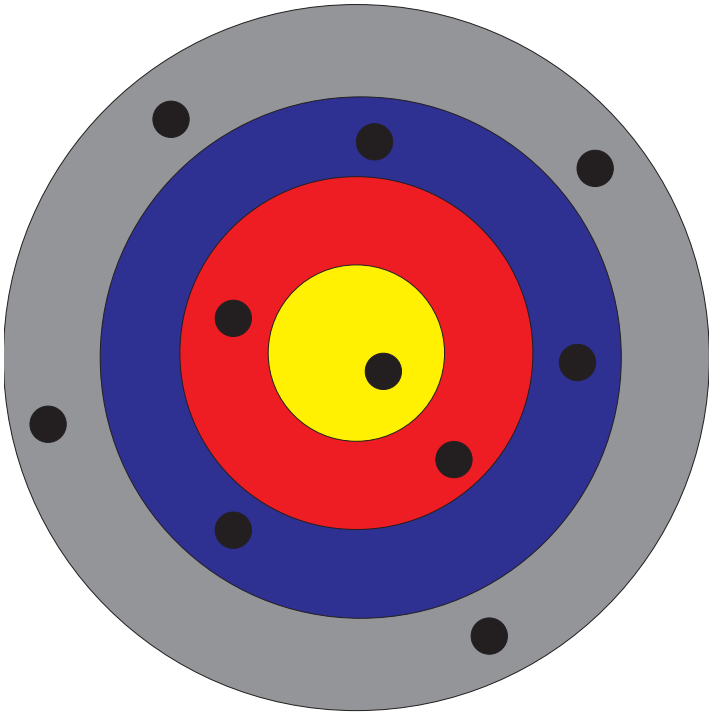

Archers shoot randomly at the target. The black dots describe their results. Knowing the rewards given to the archers we are able to conclude about the size of the bull's-eye of the target. Similarly, in the heavy-ion experiment we can make an estimate of the size of the overlapping region of two nuclei, if the number of the produced particles (a reward in this case) is a monotonic function of this size.

2.4 Reaction plane

In particle as well as in nuclear physics it is practical to introduce a coordinate system, where the spatial z-axis is parallel to the beam of the accelerator, and where the impact vector **b** points in x-direction. The two axes, x and z, span the **reaction plane** of a given collision.

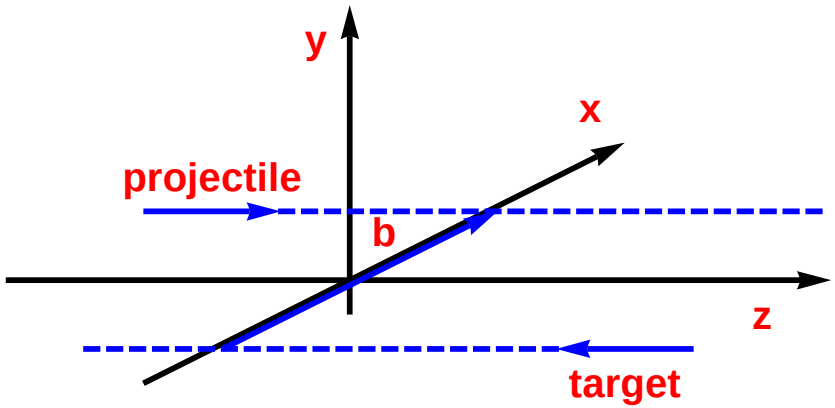

2.5 Collective flows

At present the extraction of the reaction (participant) plane is one aspect of the very advanced **flow analysis** of the collisions. In this type of the investigations one represents the momentum distribution of the produced particles in the form

$$\frac{dN}{dy d^2 p_\perp} = \frac{dN}{2\pi p_\perp dp_\perp dy}\left[1 + \sum_{k=1}^{\infty} 2 v_k \cos\left(k(\phi_p - \Psi_k)\right)\right], \tag{14}$$

where Ψ_k is the reference angle defined by the condition $\langle \sin(k\Psi_k)\rangle = 0$, where the averaging is done over all particles in one event.

Until very recently it has been common to assume $\Psi_k = \Psi_{\rm RP}$.

Averaging of (14) over the azimuthal angle gives the transverse-momentum distribution (4). The coefficients v_k characterize the momentum anisotropy. The coefficient v_1 is called the **directed flow**, whereas the coefficient v_2 is called the **elliptic flow**. In general, the coefficients v_k are functions of rapidity and transverse momentum, $v_k = v_k(y, p_\perp)$, and in this form often called the kth harmonic **differential flow**.

2.5.1 Collective flows: directed flow

Schematic view of the directed flow observed at relativistic energies. For positive and large rapidities ($y \sim y_P$) the spectators are deflected towards positive values of x. For positive and small rapidities ($y \geq 0$) the produced particles have negative v_1, hence they are deflected towards negative values of x.

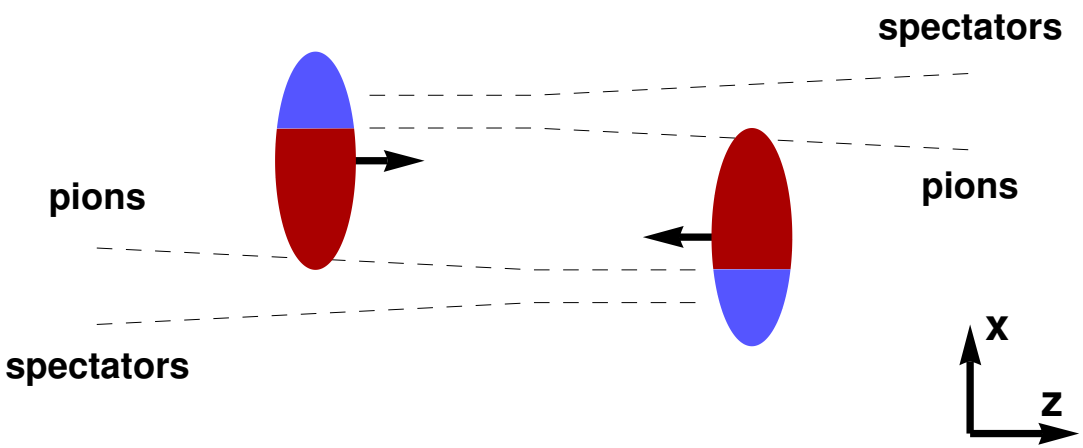

2.5.2 Collective flows: elliptic flow

In non-central collisions the region of the particle production has an almond shape in the transverse plane. Due to the interaction of the produced particles the spatial asymmetry leads to the azimuthal asymmetry of the momentum distributions. At ultra relativistic energies, the expansion is stronger in the reaction plane — the produced matter is not blocked by spectators.

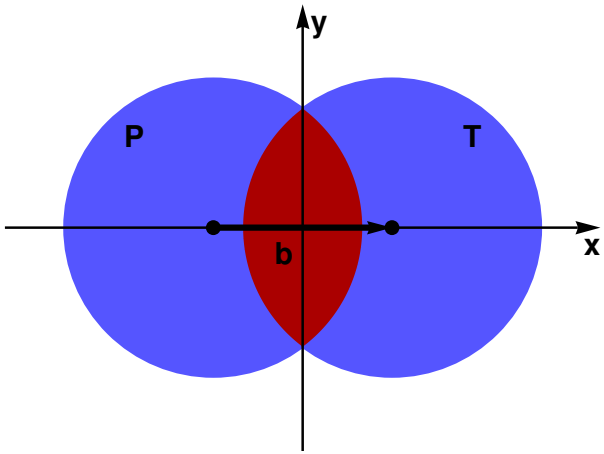

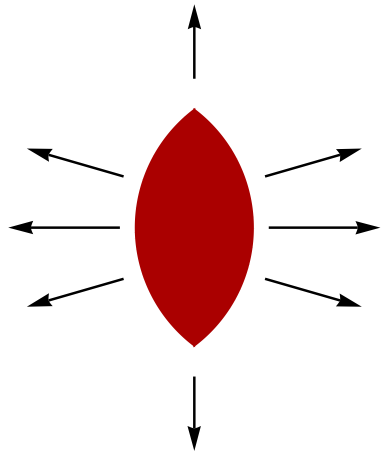

2.6 Stopping and transparency

The relativistic heavy-ion collisions can proceed in two different ways. In the collisions with large **stopping power** the baryons from the colliding nuclei are stopped in the middle of the reaction zone, and a dense baryon-rich matter is produced at midrapidity. On the other hand, in the **transparent** collisions (negligible stopping) the initial baryons are not slowed down, and the two baryon-rich regions are separated from each other.

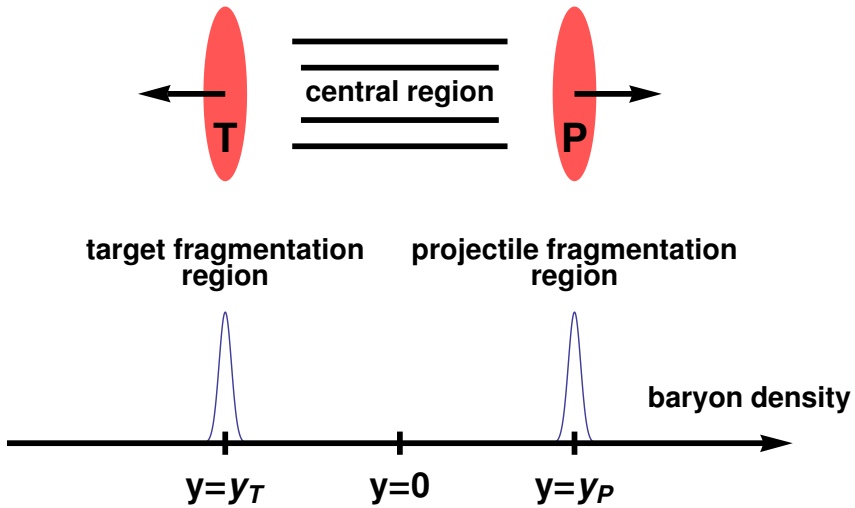

2.6 Stopping and transparency

The net-proton distributions measured in different experiments.

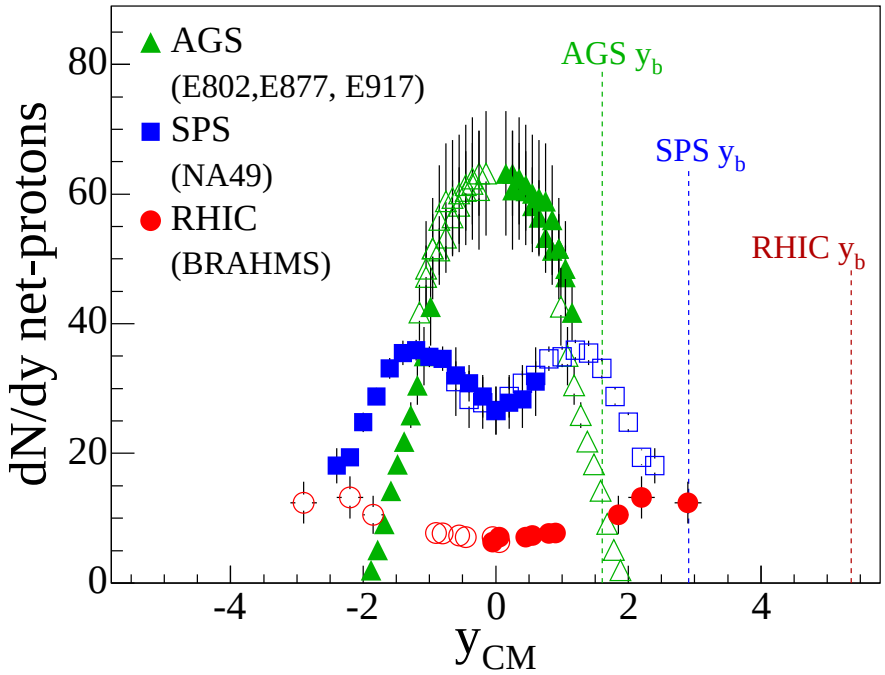

2.7 Boost invariance

Generally speaking, boost-invariance is the symmetry of the physical systems with respect to Lorentz boosts along the beam axis. It imposes special constraints on the form of the physical quantities.

For example, the thermodynamic functions used in the relativistic hydrodynamics, such as temperature, pressure, or the energy density, are Lorentz scalars. The boost-invariance in this cases means that they may depend only on the transverse coordinates and the longitudinal proper time $\tau = \sqrt{t^2 - z^2}$.

Similarly, the rapidity distribution dN/dy is boost-invariant if it is independent of rapidity. The longitudinal flow has the scaling form

$$v_z = \frac{z}{t}. \tag{15}$$

3. GLAUBER MODEL

Roy Glauber
receiving Nobel Prize
Stockholm, Dec. 2005.

In realistic situations the separation between spectators and participants is not so sharp as in the simple geometric picture introduced earlier.

A more elaborate estimate of the number of participating nucleons can be done within the **Glauber model** which **treats a nucleus-nucleus collision as a multiple nucleon-nucleon collision process**.

In the Glauber model, **the nucleon distributions in nuclei are random and given by the nuclear density profiles**

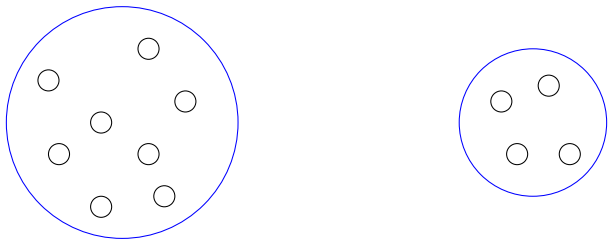

whereas the **elementary nucleon-nucleon collision is characterized by the total inelastic cross section** $\sigma_{\rm in}$.

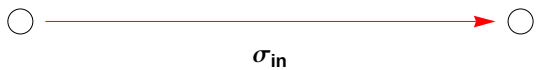

Initially, the Glauber model was applied only to elastic collisions. In this case a nucleon does not change its properties in the individual collisions, so all nucleon interactions can be well described by the same cross section.

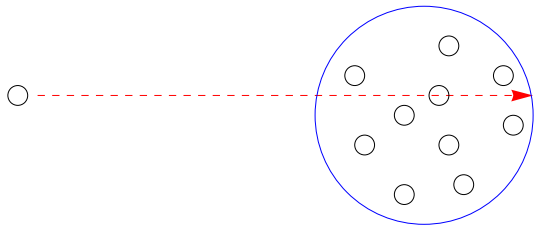

Applying the Glauber model to inelastic collisions, we assume that after a single inelastic collision an excited nucleon-like object is created that interacts basically with the same inelastic cross section with other nucleons.

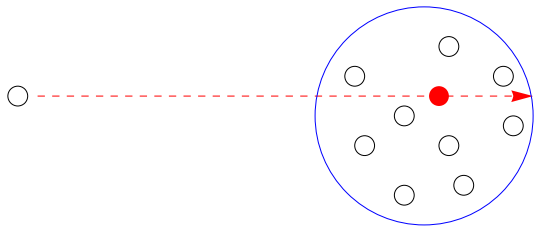

3.1 Eikonal approximation

Classical approximation to the angular momentum: after replacing l by b we may treat b as the continuous variable (with $db = dl/p$ and $d^2b = b\,db\,d\phi$). In this approximation, the scattering amplitude has the form

$$f(s,\mathbf{b}) = \frac{ip}{2\pi}\int d^2b\, e^{i\mathbf{q}\cdot\mathbf{b}}\left[1 - e^{i\chi(s,\mathbf{b})}\right], \quad \chi(s,\mathbf{b}) = 2\,\delta(s,\mathbf{b}). \tag{16}$$

The **total cross section** may be obtained from the **forward scattering amplitude** with the help of the **optical theorem**

$$\sigma_{\rm tot} = \frac{4\pi}{p}\,\mathrm{Im}\, f(s,t=0) = 2\int d^2b\,\left[1 - \mathrm{Re}\, e^{i\chi(s,\mathbf{b})}\right]. \tag{17}$$

3.1 Eikonal approximation

The **elastic cross section** is obtained by squaring the amplitude and integrating over the solid angle. Since the scattering is concentrated in the forward direction, the integration over the solid angle may be replaced by the integral over the space orthogonal to the momentum vector **p**,

$$d\Omega = \frac{d^2q}{p^2}. \tag{18}$$

Using this property we obtain

$$\begin{aligned} \sigma_{\rm el} &= \int \frac{d^2q}{4\pi^2} \int d^2b \int d^2b' e^{i\mathbf{q}\cdot\mathbf{b}} \left[1 - e^{i\chi(s,\mathbf{b})}\right] e^{-i\mathbf{q}\cdot\mathbf{b}'} \left[1 - e^{i\chi(s,\mathbf{b}')}\right]^* \\ &= \int d^2b \left|1 - e^{i\chi(s,\mathbf{b})}\right|^2. \end{aligned} \tag{19}$$

Finally, the **inelastic cross section** is

$$\sigma_{\rm in} = \sigma_{\rm tot} - \sigma_{\rm el} = \int d^2b \left(1 - \left|e^{i\chi(s,\mathbf{b})}\right|^2\right) \equiv \int d^2b\, p(\mathbf{b}). \tag{20}$$

3.2.2 Nucleon-nucleon collisions: thickness function

Let us consider a nucleon-nucleon collision at a given energy $\sqrt{s}$ and at an impact parameter b. According to our discussion presented before, we may introduce the **probability of having a nucleon-nucleon inelastic collision**

$$p(\mathbf{b}) = \left(1 - \left|e^{i\chi(\mathbf{b})}\right|^2\right) \equiv t(\mathbf{b})\,\sigma_{\rm in}. \tag{21}$$

The function $t(\mathbf{b})$, defined by (21), is called the nucleon-nucleon **thickness function**. The integral of $p(\mathbf{b})$ over the whole range of the impact parameter should be normalized to $\sigma_{\rm in}$. Thus, the thickness function is normalized to unity

$$\int d^2b\, t(\mathbf{b}) = 1. \tag{22}$$

For collisions with unpolarized beams $t(\mathbf{b})$ depends only on the magnitude of $\mathbf{b}$.

3.3.1 Nucleon-nucleus collisions: density profiles

The probability of finding a nucleon in the nucleus with the atomic mass number A is the usual baryon density divided by the number of baryons in the nucleus (our definition of $\rho_A(r)$ includes A in the denominator, because we want to interpret $\rho_A(r)$ as the probability distribution.). For large nuclei, one commonly uses the **Woods-Saxon function**

$$\rho_A(r) = \frac{\rho_0}{A\left(1+\exp\left[\frac{r-r_0}{a}\right]\right)}, \tag{23}$$

with the parameters:

$$r_0 = (1.12A^{1/3} - 0.86A^{-1/3})\,\mathrm{fm}, \tag{24}$$

$$a = 0.54\,\mathrm{fm}, \tag{25}$$

and

$$\rho_0 = 0.17\,\mathrm{fm}^{-3}. \tag{26}$$

The parameter ρ_0 is the **nuclear saturation density**.

3.3.1 Nucleon-nucleus collisions: density profiles

The **nucleon-nucleus thickness function** for the nucleus A is obtained from a simple geometric consideration (see right) and the assumption that the nucleon positions in the nucleus A are not changed during the collision process,

$$T_A(\mathbf{b}) = \int dz_A \int d^2 s_A \, \rho_A(\mathbf{s}_A, z_A) \, t(\mathbf{s}_A - \mathbf{b}). \tag{27}$$

Here the transverse coordinates are denoted by the vector $\mathbf{s}_A$, and we use notation

$$\rho_A(\mathbf{s}_A, z_A) = \rho_A\left(\sqrt{\mathbf{s}_A^2 + z_A^2}\right). \tag{28}$$

Equation (22) implies the normalization condition

$$\int d^2 b \, T_A(\mathbf{b}) = 1. \tag{29}$$

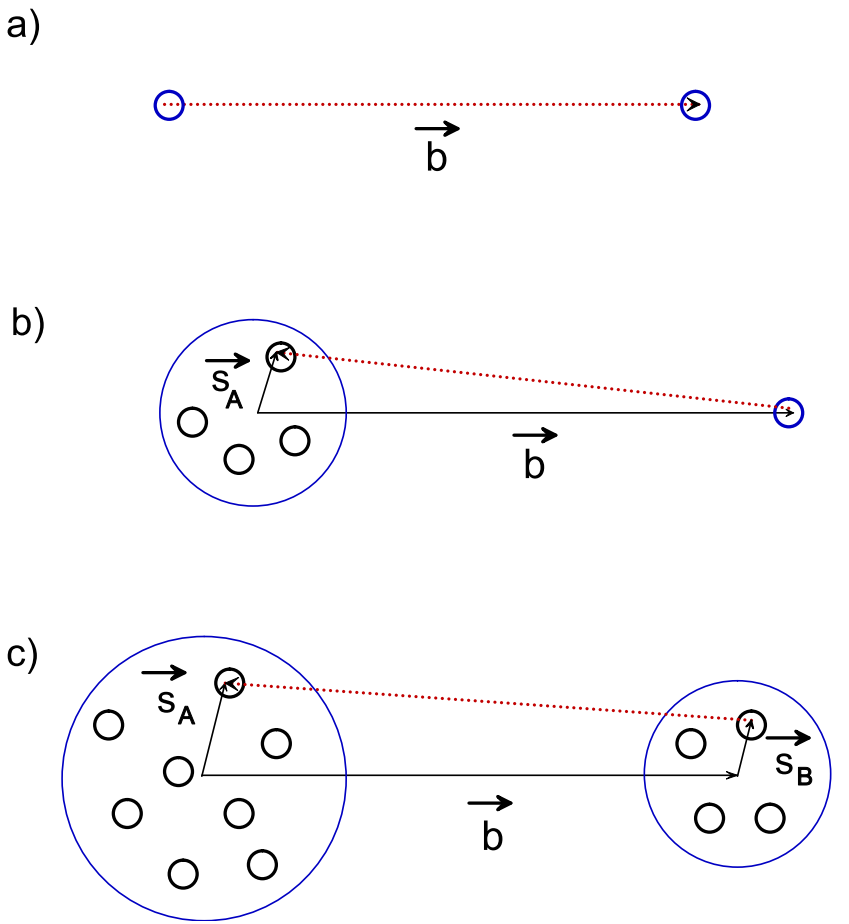

3.3.2 Nucleon-nucleus collisions: independent collisions

The quantity $T_A(\mathbf{b})\,\sigma_{\rm in}$ is the probability that a single nucleon-nucleon collision takes place in a nucleon-nucleus collision at the impact parameter **b**. Treating all possible nucleon-nucleon collisions in the nucleon-nucleus collision as completely independent and characterized by the same cross section, we easily find the probability of having n such collisions. The latter is expressed by the binomial distribution

$$P(n;A;\mathbf{b}) = \left(\begin{array}{c} A \\ n \end{array} \right) [1 - T_A(\mathbf{b})\,\sigma_{\rm in}]^{A-n} [T_A(\mathbf{b})\,\sigma_{\rm in}]^n . \tag{30}$$

The **average number of binary nucleon-nucleon collisions** may be calculated from (30) which gives

$$\overline{n}(A;\mathbf{b}) = \sum_{n=1}^{A} nP(n;A;\mathbf{b}) = A\,T_A(\mathbf{b})\;\sigma_{\rm in}. \tag{31}$$

3.3.2 Nucleon-nucleus collisions: independent collisions

Since the scale at which the nucleon-nucleon thickness function varies is typically smaller than the scale at which the nuclear density changes, we may often replace $t(\mathbf{s}_A - \mathbf{b})$ in (27) by the delta function $\delta^{(2)}(\mathbf{s}_A - \mathbf{b})$. In this approximation $T_A(\mathbf{b})$ is the nuclear density projected onto the transverse plane

$$T_A(\mathbf{b}) = \int dz_A \, \rho_A(\mathbf{b}, z_A), \tag{32}$$

and the average number of the collisions is

$$\overline{n}(A; \mathbf{b}) = A \, \sigma_{\mathrm{in}} \int dz_A \, \rho_A(\mathbf{b}, z_A). \tag{33}$$

3.4 Nucleus-nucleus collisions

Finally, we define the thickness function for the nucleus-nucleus collision. A geometric consideration leads to the formula

$$T_{AB}(\mathbf{b}) = \int dz_A \int d^2 s_A \, \rho_A(\mathbf{s}_A, z_A) \int dz_B \int d^2 s_B \, \rho_B(\mathbf{s}_B, z_B) \, t(\mathbf{b} + \mathbf{s}_B - \mathbf{s}_A), \tag{34}$$

with the corresponding normalization condition

$$\int d^2 b \, T_{AB}(\mathbf{b}) = 1. \tag{35}$$

The quantity $T_{AB}(\mathbf{b})\,\sigma_{\rm in}$ is the **averaged** probability that a nucleon-nucleon collision takes place in a nucleus-nucleus collision characterized by the impact parameter **b**. In the limit $t(\mathbf{b}) \to \delta^{(2)}(\mathbf{b})$ we may write

$$T_{AB}(\mathbf{b}) = \int d^2 s_A \, T_A(\mathbf{s}_A) \, T_B(\mathbf{s}_A - \mathbf{b}). \tag{36}$$

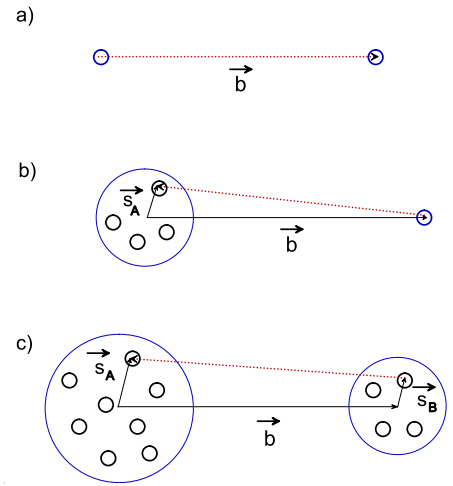

3.4 Nucleus-nucleus collisions

In a more symmetric form we have

$$T_{AB}(\mathbf{b}) = \int d^2 s \, T_A\left(\mathbf{s} + \frac{1}{2}\mathbf{b}\right) \, T_B\left(\mathbf{s} - \frac{1}{2}\mathbf{b}\right). \tag{37}$$

The nucleus-nucleus thickness function $T_{AB}(\mathbf{b})$ can be used to calculate the probability of having n inelastic binary nucleon-nucleon collisions in a nucleus-nucleus collision at the impact parameter $\mathbf{b}$.

$$P(n; AB; \mathbf{b}) = \left(\begin{array}{c} AB \\ n \end{array} \right) [1 - T_{AB}(\mathbf{b})\, \sigma_{\mathrm{in}}]^{AB-n} \, [T_{AB}(\mathbf{b})\, \sigma_{\mathrm{in}}]^n . \tag{38}$$

The result for the average number of the collisions is

$$\overline{n}(AB; \mathbf{b}) = AB \, T_{AB}(\mathbf{b}) \, \sigma_{\mathrm{in}}. \tag{39}$$

3.4.1 ... total inelastic cross section

The total probability of an inelastic nuclear collision is the sum over n from $n = 1$ to $n = AB$

$$P_{\rm in}\left(AB;\mathbf{b}\right) = \sum_{n=1}^{AB} P\left(n;AB;\mathbf{b}\right) = 1 - \left[1 - T_{AB}\left(\mathbf{b}\right)\sigma_{\rm in}\right]^{AB}. \tag{40}$$

From (40), by integrating over the impact parameter space, one may obtain the **total inelastic cross section for the collision of the two nuclei** A **and** B

$$\sigma_{\rm in}^{AB} = \int d^2b \left(1 - \left[1 - T_{AB}\left(\mathbf{b}\right)\sigma_{\rm in}\right]^{AB}\right). \tag{41}$$

Using the thickness function for the Au+Au collisions we find $\sigma_{\rm in}^{\rm AuAu}$ = 6.8 b for $\sigma_{\rm in}$ = 30 mb and $\sigma_{\rm in}^{\rm AuAu}$ = 7.0 b for $\sigma_{\rm in}$ = 40 mb. We note that those cross sections are larger than the geometric cross section $\sigma_{\rm geo}^{\rm AuAu} = 4\pi R^2 \approx 5\pi A^{2/3}$ = 5.3 b. This is due to the tails of the Woods-Saxon distribution (23), which make possible that a nucleon-nucleon collision occurs in the nuclear collision at the impact parameter b larger than $2R$.

3.4.1 ... total inelastic cross section

We did something wrong! We used the averaged probability for nucleon-nucleon collisions! In more realistic calculations, the positions of nucleons in the target and projectile nucleus are fixed, and the averaging is done later. The probability of an inelastic collision for a fixed nucleon configuration equals

$$1-\prod_{j=1}^{A}\prod_{i=1}^{B}\left[1-t\left(\mathbf{b}+\mathbf{s}_i^B-\mathbf{s}_j^A\right)\sigma_{\rm in}\right]. \tag{42}$$

The probability of an inelastic **nuclear collision** at the impact parameter **b** is then

$$\begin{aligned} P_{\rm in}\left(AB;\mathbf{b}\right) \;=\; & \int d^2s_1^A T_A(\mathbf{s}_1^A)\cdots d^2s_A^A T_A(\mathbf{s}_A^A)\int d^2s_1^B T_B(\mathbf{s}_1^B)\cdots d^2s_B^B T_B(\mathbf{s}_B^B) \\ & \times\left\{1-\prod_{j=1}^{A}\prod_{i=1}^{B}\left[1-t\left(\mathbf{b}+\mathbf{s}_i^B-\mathbf{s}_j^A\right)\sigma_{\rm in}\right]\right\}. \end{aligned} \tag{43}$$

The integration of (43) over b gives $\sigma_{\rm in}^{AB}$. Equations (40) and (43) differ from each other! The more accurate formula (43) is much more complicated to handle and cannot be simply reduced to (40). Only for nucleon-nucleus collisions the two methods are equivalent. Since there is no good analytic method to evaluate (43) for large values of A and B, one is most often satisfied with Eqs. (40) and (41) only. These equations are called the **optical limit of the Glauber model**.

3.5 Wounded nucleons

The Glauber model can be used also to calculate the number of the participants. To be more precise we distinguish between the **participants which may interact elastically** and the **participants which interact only inelastically**. The latter are called the **wounded nucleons**.

The number of nucleons in the nucleus A

$$A \int d^2 s \, T_A(\mathbf{s}). \tag{44}$$

Probability, that the nucleus from A at the position $\mathbf{s}$ collides one or more times with the nucleons in B (in an AB collision at the impact parameter $\mathbf{b}$)

$$\sum_{n=1}^{B} P\left(n; B; \mathbf{b}-\mathbf{s}\right) = 1 - \left[1 - \sigma_{\mathrm{in}} T_B\left(\mathbf{b}-\mathbf{s}\right)\right]^B . \tag{45}$$

The number of wounded nucleons in A is

$$\overline{w}_A\left(A; B; \mathbf{b}\right) \quad = \quad A \int d^2 s \, T_A\left(\mathbf{s}\right) \left(1 - \left[1 - \sigma_{\mathrm{in}} T_B\left(\mathbf{b}-\mathbf{s}\right)\right]^B\right). \tag{46}$$

3.5 Wounded nucleons

Similarly, the number of wounded nucleons in B is

$$\overline{w}_B(A;B;\mathbf{b}) = B\int d^2s\, T_B(\mathbf{s})\left(1-[1-\sigma_{\rm in}T_A(\mathbf{b}+\mathbf{s})]^A\right). \quad (47)$$

Since the number of wounded nucleons in the collision of A and B is the sum of the wounded nucleons in the nucleus A and B, we obtain (after making the appropriate shifts in the integration over positions $\mathbf{s}$)

$$\begin{aligned}\overline{w}(A;B;\mathbf{b}) = & A\int d^2s\, T_A(\mathbf{b}-\mathbf{s})\left(1-[1-\sigma_{\rm in}T_B(\mathbf{s})]^B\right)\\ & + B\int d^2s\, T_B(\mathbf{b}-\mathbf{s})\left(1-[1-\sigma_{\rm in}T_A(\mathbf{s})]^A\right). \quad (48)\end{aligned}$$

3.5.1 Wounded nucleons vs. binary collisions

The numbers of binary collisions, $\overline{n}(b)$, and the numbers of wounded nucleons, $\overline{w}(b)$, for Au+Au collisions ($A = 197$) at different values of the impact parameter b. The results are presented for two different values of the nucleon-nucleon inelastic cross section: $\sigma_{\rm in}$ = 30 mb (the second and the third column), and $\sigma_{\rm in}$ = 40 mb (the fifth and the sixth column). The fourth and seventh columns give geometric estimates of the centrality class of the collisions with the impact parameters **smaller** than b (the fourth column is for $\sigma_{\rm in}^{\rm AuAu}$ = 6.8 b, whereas the sixth column is for $\sigma_{\rm in}^{\rm AuAu}$ = 7.0 b).

b [fm]	$\overline{n}(b)$	$\overline{w}(b)$	c	$\overline{n}(b)$	$\overline{w}(b)$	c
0	881	370	0.00	1174	378	0.00
1	859	363	0.00	1146	371	0.00
2	801	344	0.02	1068	354	0.02
3	717	315	0.04	957	326	0.04
4	617	280	0.07	823	291	0.07
5	587	241	0.12	783	251	0.11
6	397	200	0.17	530	211	0.16
7	298	160	0.23	397	170	0.22
8	209	122	0.29	279	131	0.29
9	136	88	0.37	182	95	0.36
10	82	58	0.46	109	64	0.45

3.6 Soft and hard processes

It is an experimental fact that pions (the most abundant particles produced in a nucleon-nucleon as well as in a nucleus-nucleus collision) have on average small transverse momenta, $p_\perp \sim 400$ MeV. The processes leading to the production of such low-energetic pions are called **soft processes**. On the other hand, the pions with large transverse momenta, $p_\perp > 1$–2 GeV, are produced by **hard processes**.

The soft processes cannot be described directly by perturbative QCD. In this case the strong coupling constant is large and the nonperturbative effects, which are very difficult to deal with, are important. Contrary, the hard processes involve large momentum transfers connected with a small value of the strong coupling constant. Hence, they can be described successfully by the methods of perturbative QCD.

3.6 Soft and hard processes

Can we use the knowledge of $\overline{w}_{AB}$ and $\overline{n}_{AB}$ to make an estimate of the multiplicity of the particles produced in a nuclear collision, provided the information about the multiplicity of the particles produced in a more elementary nucleon-nucleon collision (at the same energy) is available?

SEARCH FOR SIMPLE SCALINGS (SUPERPOSITION RULES)

For hard processes it is natural to assume that the number of the produced particles scales with the number of binary collisions. In this case the scattering processes are well localized and the interference effects between different collisions may be neglected. For soft processes the appropriate scaling is more difficult to find. In fact, it is a postulate of the wounded-nucleon model that the multiplicity of soft particles scales with the number of the wounded nucleons.

3.7 Wounded-nucleon model

Białas, Bleszyński and Czyż argued (in 1976) that the average multiplicity in a collision of two nuclei with the mass numbers A and B is

$$\overline{N}_{AB} = \frac{1}{2}\,\overline{w}_{AB}\,\overline{N}_{\mathrm{NN}}, \tag{49}$$

where $\overline{N}_{\mathrm{NN}}$ is the average multiplicity in proton-proton (nucleon-nucleon) collisions, and $\overline{w}_{AB}$ is the average number of the wounded nucleons (calculated in the Glauber framework). The energy dependence of $\overline{N}_{\mathrm{NN}}$ is described by (**??**). The motivation for the use of (49) came from the interpretation of the nucleon-nucleus interactions. The formula (49) with an additional expression for the dispersion of multiplicity distributions form the main ingredients of the **wounded-nucleon model** of the nucleus-nucleus collisions.

3.7 Wounded-nucleon model

The charged particle pseudorapidity density as a function of the number of the participants. The measurement of the PHENIX group at RHIC, $\sqrt{s_{\mathrm{NN}}}$ = 130 GeV, is compared to the measurement done by the WA98 group at the SPS, $\sqrt{s_{\mathrm{NN}}}$ = 17.3 GeV.

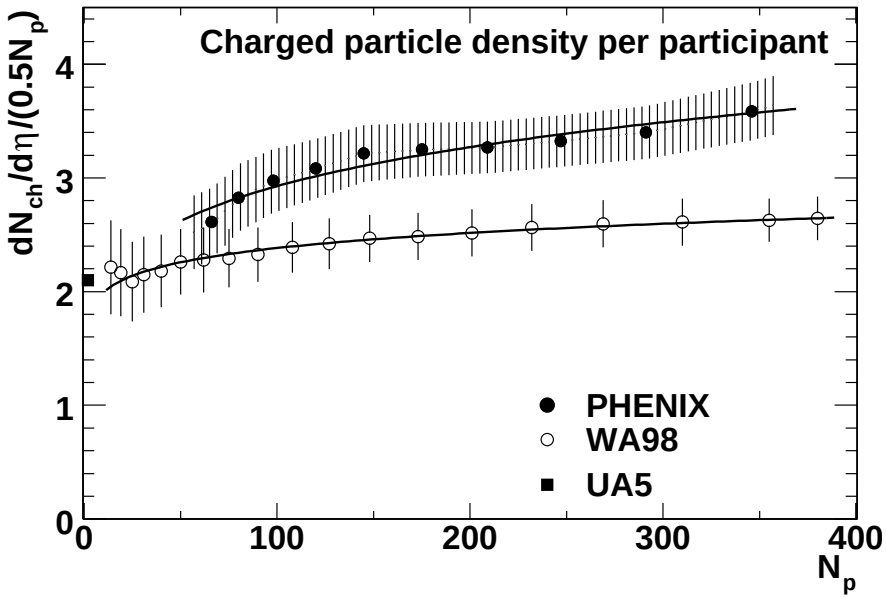

3.8 Nuclear modification factor

A simple way to quantify the differences between the nucleus-nucleus collisions and the nucleon-nucleon collisions is to calculate the **nuclear modification factor**,

$$R_{AB}(p_\perp) = \frac{1}{\overline{n}_{AB}} \frac{d^2\overline{N}_{AB}}{dp_\perp d\eta} \Big/ \frac{1}{\sigma^{pp}_{\rm tot}} \frac{d\sigma^{pp}_{\rm incl}}{dp_\perp d\eta}. \tag{50}$$

$\overline{N}_{AB}$ – average number of particles produced in the collisions of the nuclei A and B, $\overline{n}_{AB}$ – number of the binary nucleon-nucleon collisions obtained in the framework of the Glauber model.

The denominator of (50) is the inclusive cross section for pp collisions divided by the total cross section. This quantity is equal to the average number of particles produced in pp collisions in the appropriate phase-space interval,

$$\frac{dN_{pp}}{dp_\perp d\eta} = \frac{1}{\sigma^{pp}_{\rm tot}} \frac{d\sigma^{pp}_{\rm incl}}{dp_\perp d\eta}. \tag{51}$$

If the collisions of the nuclei A and B are simple superpositions of the elementary pp collisions, the scaling with the number of binary collisions should hold, and the nuclear modification factor is expected to be equal to 1.

3.8 Nuclear modification factor

The nuclear modification factor R_{dAu} as measured by the PHOBOS Collaboration at BNL.

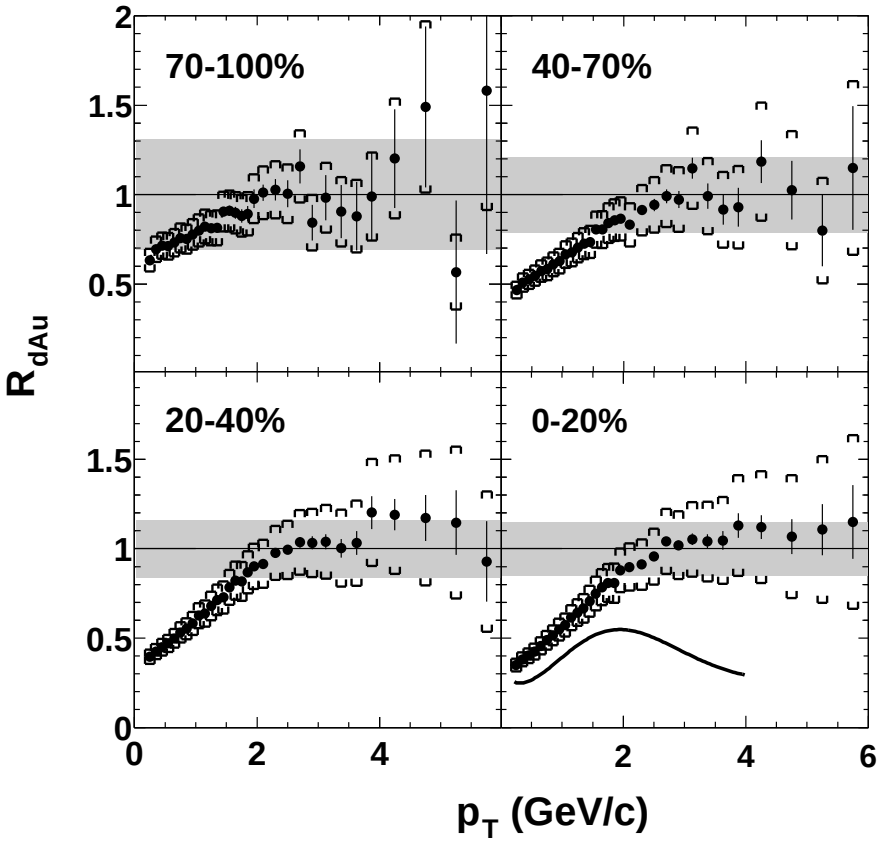

3.8 Nuclear modification factor

The nuclear modification factors R_{AuAu} for central and peripheral collisions (the upper and central two panels), and their ratio (the lower two panels). The measurement of the BRAHMS Collaboration at BNL.

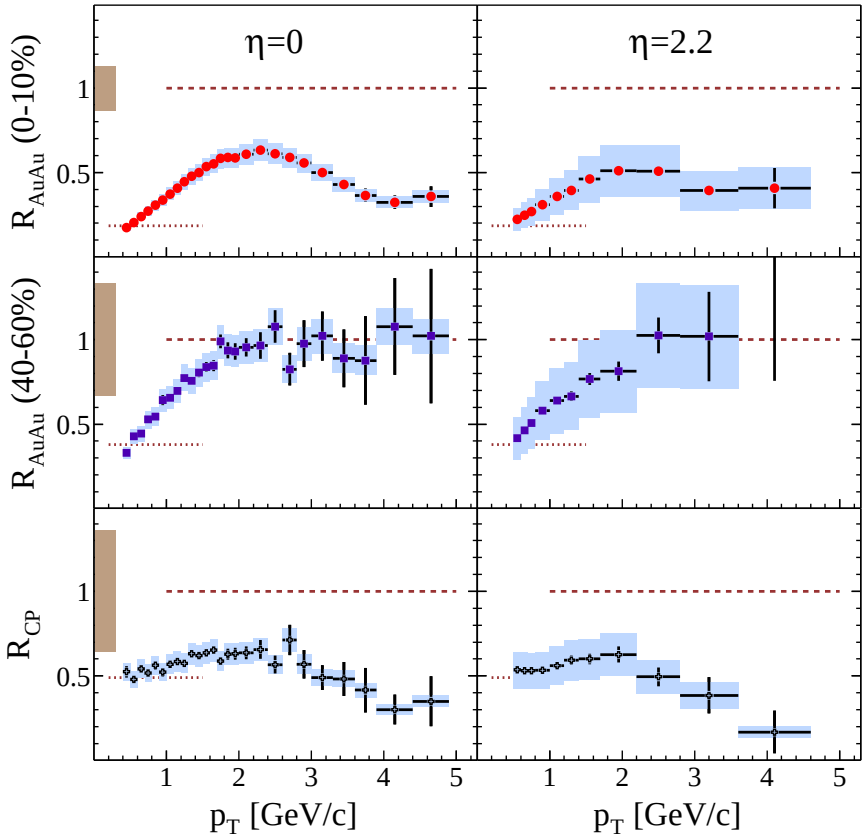

3.8 Nuclear modification factor

The nuclear modification factors R_{dAu} and R_{AuAu} measured by the PHENIX Collaboration at BNL.

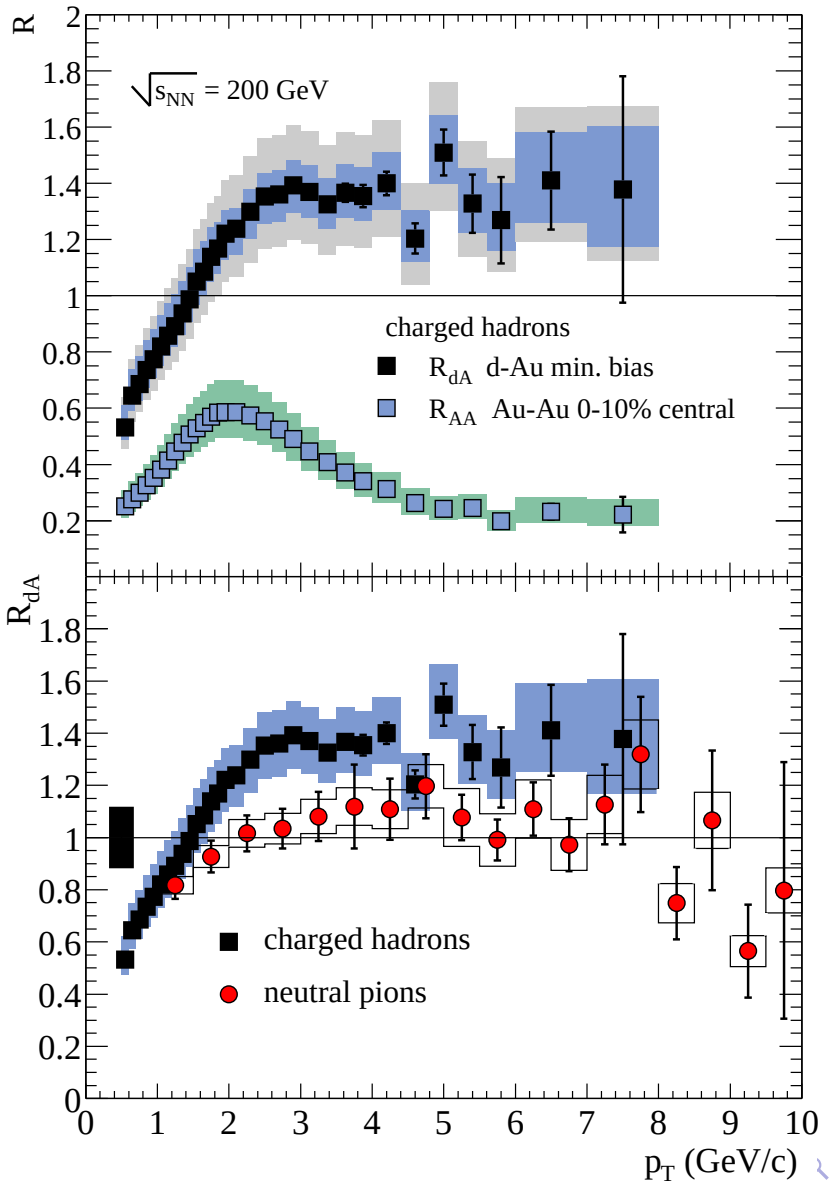

4. SPACE-TIME PICTURE OF ULTRA-RELATIVISTIC HEAVY-ION COLLISIONS

The spacetime diagram of ultra-relativistic nuclear collisions. In the center-of-mass frame, partons moving fast hadronize later than those moving slowly. Consequently, at very high energies the evolution of the system at midrapidity is governed by the **longitudinal proper time** $\tau = \sqrt{t^2 - z^2}$, rather than by the ordinary time t. Note, that this picture breaks in the fragmentation regions (i.e., at large values of $|\eta|$) where physical processes have different character.

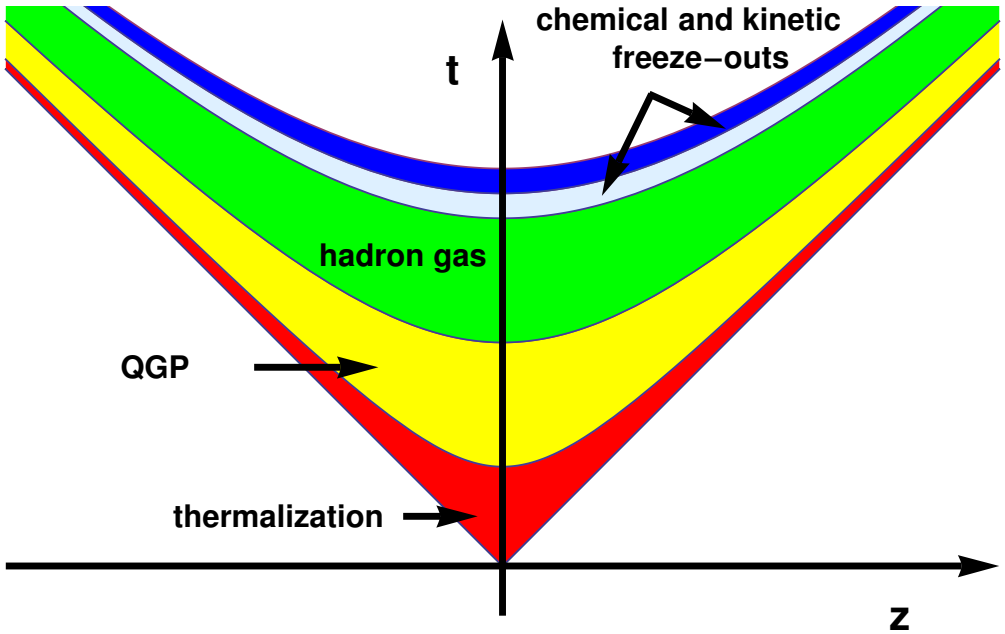

4.1 Particle production processes

The result of the multiple nucleon-nucleon collisions discussed before is that the two colliding nuclei evolve rapidly into an extended, hot and dense system of quarks and gluons.

There exist several frameworks to describe this transition, for example:

1) **QCD string breaking**,
2) **parton cascades models**,
3) **color glass condensate** evolving into **glasma** and later into the **quark-gluon plasma**.

In all cases, the process of the particle production may be characterized by the **decoherence time** $\tau_{\rm dec}$ which is required to form the incoherent distribution of quarks and gluons from the highly coherent nuclear wave functions.

Theoretical interpretations of the data measured at RHIC suggest that this time is very short, $\tau_{\rm dec} \ll 1$ fm. This is so, because the decoherence time $\tau_{\rm dec}$ should be smaller than the **equilibration time** $\tau_{\rm therm}$, and the latter has been found to be a fraction of a fermi at RHIC.

string models = soft processes

parton cascades = hard processes

4.2 Thermalization

The experimental data obtained in the RHIC experiments favor a very short thermalization/equilibration time, $\tau_{\rm therm} < 1$ fm. The **support for this idea comes mainly from applications of relativistic hydrodynamics** which successfully describes the data if one assumes an early starting time of hydro $\tau_{\rm i} < 1$ fm ($\tau_{\rm therm} \leq \tau_{\rm i}$).

Since the final multiplicities are are determined mainly by the number of wounded nucleons, it is reasonable to assume that the initial entropy density of the thermalized system is proportional to the density of wounded nucleons.

$$\sigma_{\rm i}(\mathbf{x}_\perp) \propto \overline{w}\,(\mathbf{x}_\perp)$$

4.2 Thermalization: initial conditions for hydrodynamics

The typical arrangement of the coordinate system in the transverse plane. The impact vector, denoted by the dashed arrow, lies in the reaction plane along the x-axis, $\mathbf{b} = (b, 0)$.

The center of the nucleus B has the coordinates $(b/2, 0)$,
while the center of the nucleus A is located at $(-b/2, 0)$.

The position of the wounded nucleon is given by the two-dimensional vector $\mathbf{x}_\perp = (x, y)$.

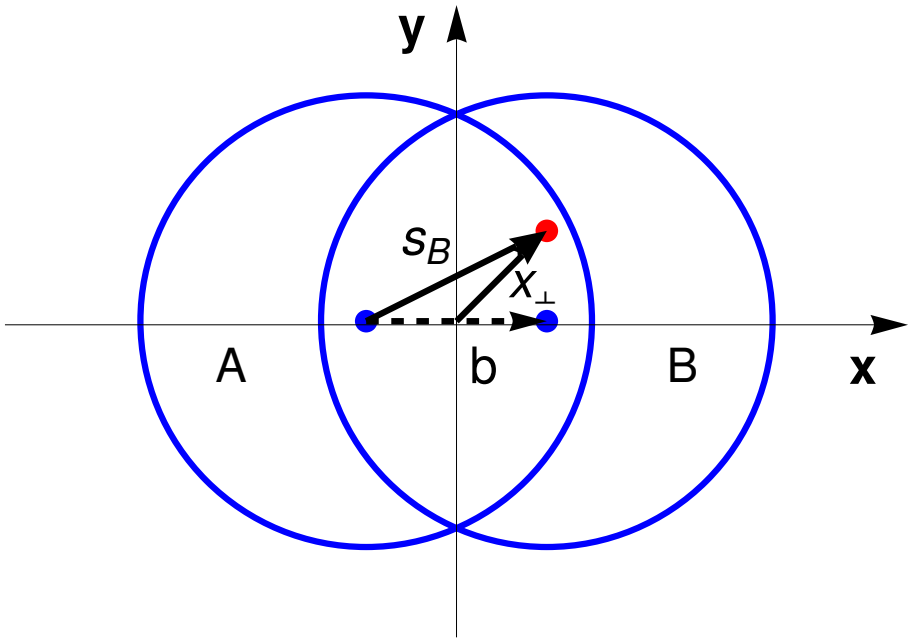

4.2 Thermalization: initial conditions for hydrodynamics

The average density of the wounded nucleons in the nucleus B at the transverse position $\mathbf{x}_\perp$ is

$$\overline{w}_B(\mathbf{x}_\perp) = B\,T_B\left(-\frac{\mathbf{b}}{2}+\mathbf{x}_\perp\right)\left\{1-\left[1-\sigma_{\rm in}\,T_A\left(\frac{\mathbf{b}}{2}+\mathbf{x}_\perp\right)\right]^A\right\}. \tag{52}$$

The average density of the wounded nucleons in the nucleus A is analogous

$$\overline{w}_A(\mathbf{x}_\perp) = A\,T_A\left(\frac{\mathbf{b}}{2}+\mathbf{x}_\perp\right)\left\{1-\left[1-\sigma_{\rm in}\,T_B\left(-\frac{\mathbf{b}}{2}+\mathbf{x}_\perp\right)\right]^B\right\}. \tag{53}$$

For the collision of two nuclei, $A+B$, one may use the final expression in the form

$$\overline{w}(\mathbf{x}_\perp) \quad = \quad \overline{w}_A(\mathbf{x}_\perp)+\overline{w}_B(\mathbf{x}_\perp). \tag{54}$$

In the case of the binary collisions, similar geometrical considerations lead to the formula

$$\overline{n}(\mathbf{x}_\perp) = \sigma_{\rm in}\,A\,B\,T_A\left(\frac{\mathbf{b}}{2}+\mathbf{x}_\perp\right)T_B\left(-\frac{\mathbf{b}}{2}+\mathbf{x}_\perp\right). \tag{55}$$

We recall that $\sigma_{\rm in}$ in Eqs. (52), (53), and (55) is the nucleon-nucleon inelastic cross section.

4.2 Thermalization: initial conditions for hydrodynamics

For boost-invariant systems with vanishing baryon chemical potential one usually assumes that either the initial entropy density, $\sigma_{\rm i}(\mathbf{x}_\perp) = \sigma(\tau_{\rm i}, \mathbf{x}_\perp)$, or the initial energy density, $\varepsilon_{\rm i}(\mathbf{x}_\perp) = \varepsilon(\tau_{\rm i}, \mathbf{x}_\perp)$, are directly related to the density of **sources of particle production**, $\rho_{\rm sr}(\mathbf{x}_\perp)$.

The sources considered in this context are **wounded nucleons** or **binary collisions**. The symmetry with respect to the Lorentz boosts along the collision axis means that it is sufficient to consider all these quantities in the plane $z = 0$. In general, a mixed model is used, with a linear combination of the wounded-nucleon density $\overline{w}(\mathbf{x}_\perp)$ and the density of binary collisions $\overline{n}(\mathbf{x}_\perp)$. This leads to the two popular choices:

$$\sigma_{\rm i}(\mathbf{x}_\perp) \;\propto\; \rho_{\rm sr}(\mathbf{x}_\perp) = \frac{1-\kappa}{2}\,\overline{w}(\mathbf{x}_\perp) + \kappa\,\overline{n}(\mathbf{x}_\perp) \tag{56}$$

or

$$\varepsilon_{\rm i}(\mathbf{x}_\perp) \;\propto\; \rho_{\rm sr}(\mathbf{x}_\perp) = \frac{1-\kappa}{2}\,\overline{w}(\mathbf{x}_\perp) + \kappa\,\overline{n}(\mathbf{x}_\perp)\,. \tag{57}$$

4.2 Thermalization: tilted source

Białas and Czyż: analysis of the deuteron-gold collisions, wounded nucleons produce particles mainly in the direction of their motion

P. Bożek: this leads to a tilted source and explains negative v_1

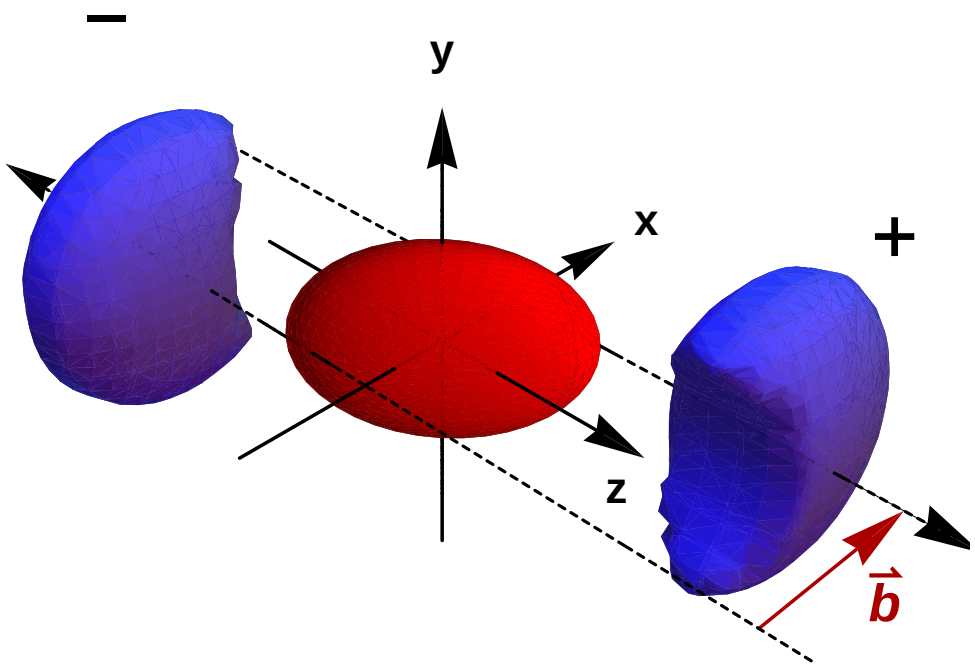

but all of this requires a hydrodynamic model of expansion...

4.3 Hydrodynamic expansion

The *perfect fluid* is defined formally by the form of its energy-momentum tensor, namely

$$T^{\mu\nu} = (\varepsilon + P)u^{\mu}u^{\nu} - Pg^{\mu\nu}, \tag{58}$$

where $g^{\mu\nu}$ is the metric tensor with $g^{00} = 1$, ε is the energy density, P is the pressure, and u^{μ} is the four-velocity of the fluid element.
Such a form of the energy-momentum tensor follows from the assumption of local thermal equilibrium. Equations of motion of the perfect fluid are obtained from the conservation laws

$$\partial_{\mu} T^{\mu\nu} = 0. \tag{59}$$

Equations of motion should be supplemented by the equation of state! Otherwise, the system of equations cannot be not closed.

4.3 Hydrodynamic expansion

For systems with non-zero baryon density n, $w = (\varepsilon + P)/n$, $s = \sigma/n$.

Substituting (58) in (59) and using thermodynamic identities gives

$$\frac{d}{d\tau}(wu^\nu) \equiv u^\mu \partial_\mu (wu^\nu) = \frac{1}{n}\partial^\nu P. \tag{60}$$

The projection of (60) on the fluid four-velocity u_ν and the use of thermodynamic identities yields

$$\frac{ds}{d\tau} \equiv u^\mu \partial_\mu s = 0. \tag{61}$$

4.4 Thermal freeze-out

The *thermal* or *kinetic freeze-out* is the stage in the evolution of matter when the hadrons practically stop to interact. In other words, the thermal freeze-out is a transition from a strongly coupled system (very likely evolving from one local equilibrium state to another) to a weakly coupled one (consisting of essentially free streaming particles).

It is triggered by the expansion of matter, which causes a rapid growth of the mean free path, λ_{mfp}, of particles. The thermal freeze-out happens when the timescale connected with the collisions, $\tau_{\mathrm{coll}} \sim \lambda_{\mathrm{mfp}}$, becomes larger than the expansion timescale, τ_{exp}. In this case the particles depart from each other so fast that the collision processes become ineffective. We may formulate this condition as the inequality

$$\tau_{\mathrm{coll}} \geq \tau_{\mathrm{exp}}. \tag{62}$$

4.4 Thermal freeze-out

The magnitude of the collision time is determined by the product of the average cross section and the particle density,

$$\tau_{\rm coll} \sim \frac{1}{\sigma\, n}, \tag{63}$$

whereas the magnitude of the expansion time is characterized by the divergence of the four-velocity field, u^μ, describing the hydrodynamic flow of matter,

$$\tau_{\rm exp} \sim \frac{1}{\partial_\mu u^\mu}\,. \tag{64}$$

Very often a simplified criterion is assumed which says that the thermal freeze-out happens at the time when the mean free path of hadrons is of the same order as the size of the system.

4.5 Chemical freeze-out

A schematic physical picture adopted in the thermal models of particle production. At a certain stage of the evolution of the system, a gas of stable hadrons and resonances is formed. The final (measured) multiplicities of hadrons consist of primary particles, present in the hot fireball, and of secondary particles coming from the decays of resonances.

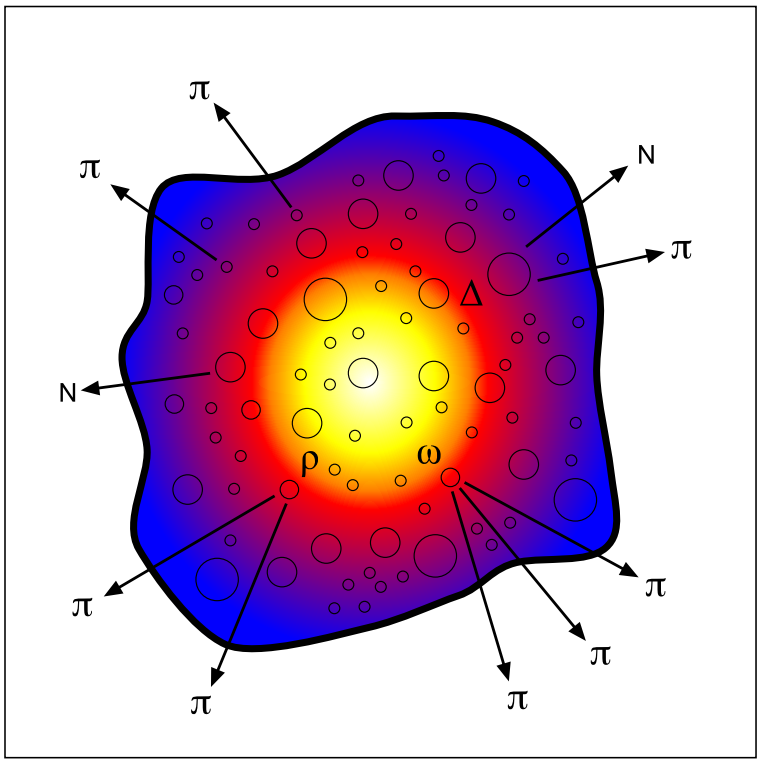

Essentially two parameters, T and μ_B explain the ratios of hadronic abundances! Great success at RHIC!

4.6 Hanbury–Brown-Twiss interferometry

The fundamental object in the HBT interferometry is the two-particle correlation function $C(\mathbf{p}_1, \mathbf{p}_2)$, measured for pairs of identical particles such as $\pi^+\pi^+$, $\pi^-\pi^-$, or K^+K^+. In general, it is defined by the expression

$$C(\mathbf{p}_1, \mathbf{p}_2) = \frac{\mathcal{P}_2(\mathbf{p}_1, \mathbf{p}_2)}{\mathcal{P}_1(\mathbf{p}_1)\mathcal{P}_1(\mathbf{p}_2)}, \tag{65}$$

where $\mathcal{P}_1(\mathbf{p})$ is the invariant inclusive one-particle distribution function in the space of rapidity and transverse-momentum,

$$\mathcal{P}_1(\mathbf{p}) = E_p \frac{dN}{d^3p} = \frac{dN}{dy d^2p_\perp}, \tag{66}$$

and $\mathcal{P}_2(\mathbf{p}_1, \mathbf{p}_2)$ is the analogous two-particle distribution

$$\mathcal{P}_2(\mathbf{p}_1, \mathbf{p}_2) = E_{p_1} E_{p_2} \frac{dN}{d^3p_1 d^3p_2} = \frac{dN}{dy_1 d^2p_{1\perp} dy_2 d^2p_{2\perp}}. \tag{67}$$

Equations (66) and (67) imply that the correlation function (65) transforms like a Lorentz scalar.

4.6 Hanbury–Brown-Twiss interferometry

In (65) we may use the average momentum

$$\mathbf{k} = \frac{1}{2}\left(\mathbf{p}_1 + \mathbf{p}_2\right), \tag{68}$$

and the difference of the two momenta

$$\mathbf{q} = \mathbf{p}_1 - \mathbf{p}_2. \tag{69}$$

The out-side-long coordinate system used in the standard HBT analysis of the correlation functions. The vector $\mathbf{k}$ lies in the $x - z$ plane. By making the Lorentz boost along the collision axis we may also set $\mathbf{k}_{||} = 0$. In this way we change to the special frame that is called the longitudinally comoving system (LCMS).

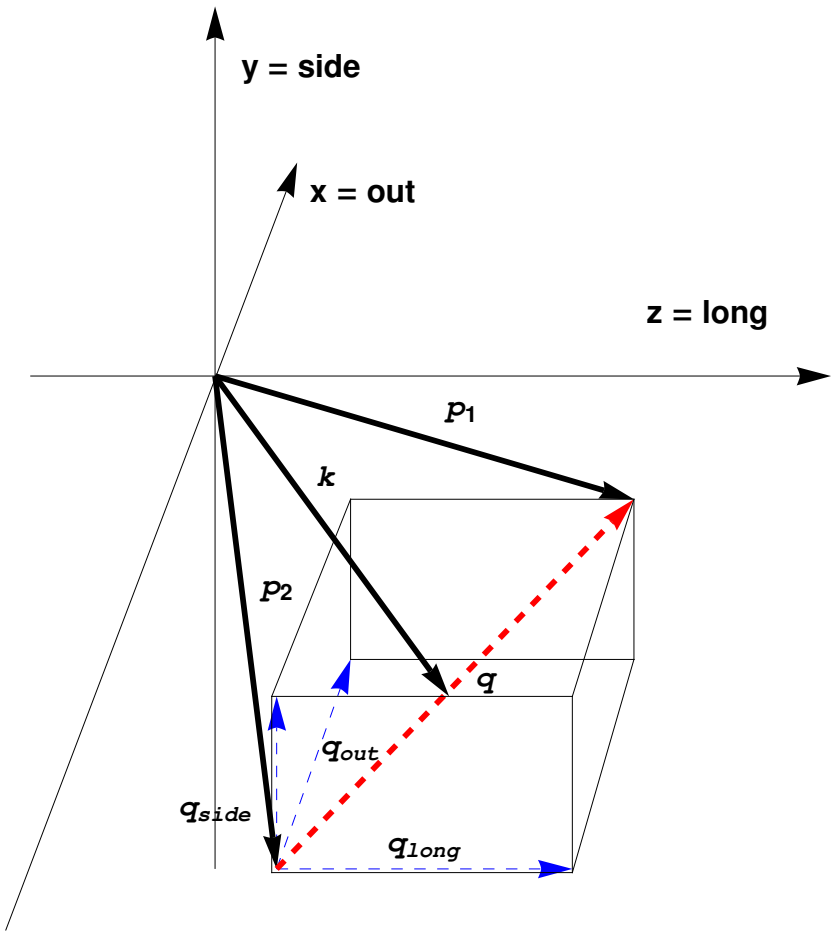

4.6 Hanbury–Brown-Twiss interferometry

$$C(k_\perp, \mathbf{q}) = 1 + \lambda \exp\left[-R^2_{\rm long}(k_\perp) q^2_{\rm long} - R^2_{\rm out}(k_\perp) q^2_{\rm out} - R^2_{\rm side}(k_\perp) q^2_{\rm side}\right]. \quad (70)$$

Pion HBT radii vs. $m_T = \sqrt{k_T^2 + m_\pi^2}$ measured by the STAR Collaboration at midrapidity in six different centrality windows.

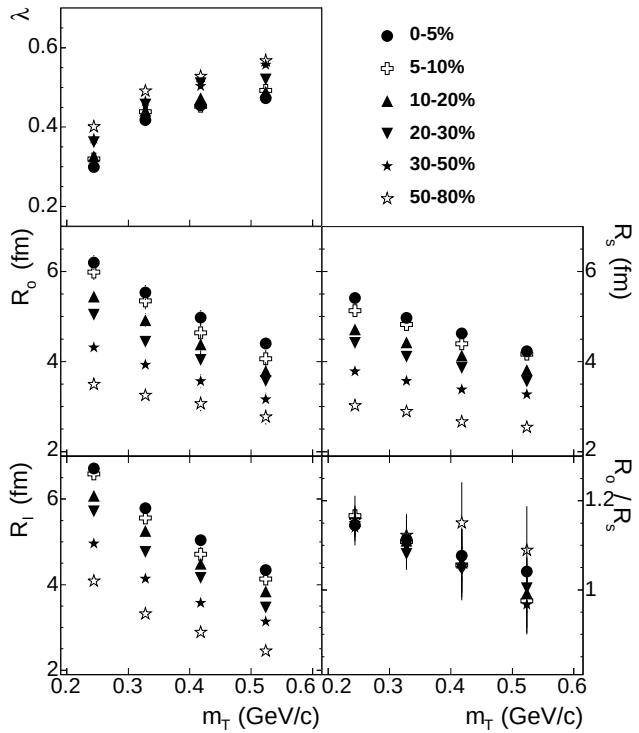

5. CONCLUSIONS

STANDARD MODEL (MODULES) of HEAVY–ION COLLISIONS

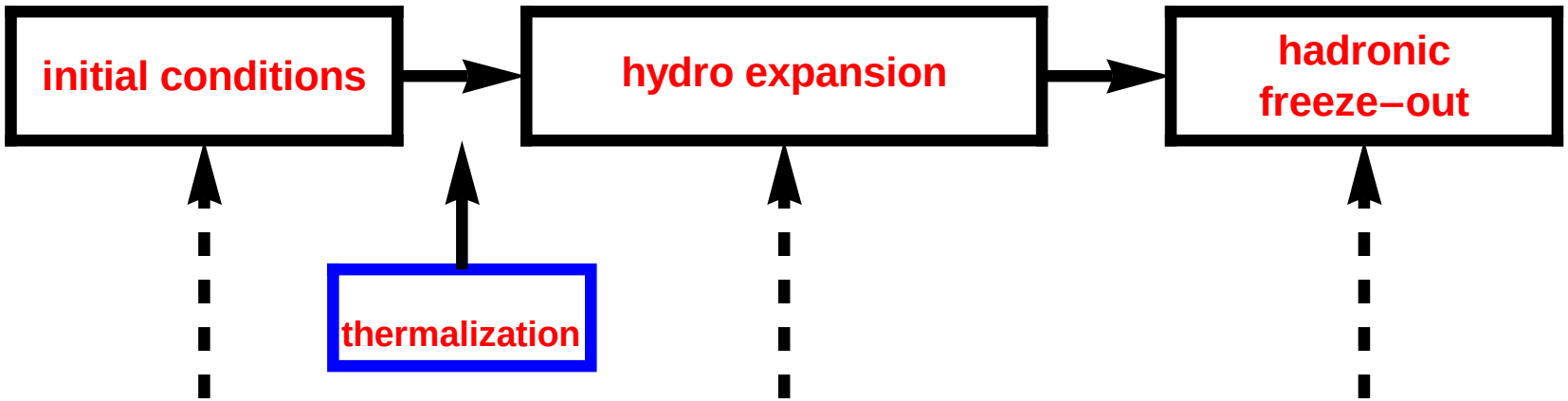

NEW: FLUCTUATIONS IN THE INITIAL STATE / EVENT–BY–EVENT HYDRO / FINAL–STATE FLUCTUATIONS

EQUATION OF STATE?

VISCOSITY?

Shuryak: *Heavy ion collisions, described well by hydro/thermodynamics, are in fact much simpler than more "elementary" pp or e+ e- collisions.*